Details of the Research Work

Title: Deciphering the Interactions and Complexation Mechanisms of flavonoids with *β*-Cyclodextrin Derivatives: Experimental Insights and Anticancer Implications

1. Introduction

Nutraceuticals have attracted significant attention in recent years due to their broad therapeutic and preventive potential [1]. Among these, genistein (GEN), a prominent isoflavone in soybeans, is known for its structural similarity to estrogen and its diverse biological activities, including cardioprotective effects, reduced risk of prostate and colon cancer, neuroprotection against Alzheimer's disease, mitigation of menopause symptoms, and treatment of non-alcoholic fatty liver disease (NAFLD) [2,3] **(Figure1).** Similarly, phloretin (PHL), a dihydrochalcone found in fruits such as apples and pears, exhibits various pharmacological effects, including the regulation of glucose transporters, antioxidant activity, and the ability to induce apoptosis in tumor cells [4,5].

Despite their promising bioactivities, both GEN and PHL suffer from poor aqueous solubility, significantly reducing their bioavailability and limiting their application in functional foods and supplements [6-8]. To overcome these limitations, cyclodextrin (CD) complexes have emerged as effective solutions to enhance the solubility, stability, and bioavailability of such hydrophobic bioactive molecules [9]. CDs are macrocyclic oligosaccharides that can encapsulate guest molecules within their hydrophobic cavities, improving their solubility and protecting them from degradation.

Among the various CDs, *β*-cyclodextrin (*β*-CD) and its modified derivatives, such as hydroxypropyl-*β*-cyclodextrin (HP-*β*-CD), methyl-*β*-cyclodextrin (M-*β*-CD), and sulfobutylether-*β*-cyclodextrin (SBE-*β*-CD, Captisol®), are particularly notable for their ability to form stable inclusion complexes with bioactive compounds. These modified CDs offer enhanced solubility, reduced toxicity, and improved binding capabilities compared to their natural counterparts [10,11].

In this study, we investigated the inclusion complexation of GEN with HP-*β*-CD and M-*β*-CD, as well as PHL with SBE-*β*-CD, to enhance their solubility and therapeutic efficacy. The inclusion complexes of GEN were prepared using the spray-drying technique, while those of PHL were produced via lyophilization **(Figure 2).** Phase solubility studies were conducted to determine the optimal molar stoichiometric ratios and encapsulation efficiencies, leading to the selection of SBE-*β*-CD for PHL and HP-*β*-CD and M-*β*-CD for GEN.

The successful formation of these inclusion complexes was confirmed through various characterization techniques, including FT-IR, Powder-XRD, SEM, and NMR

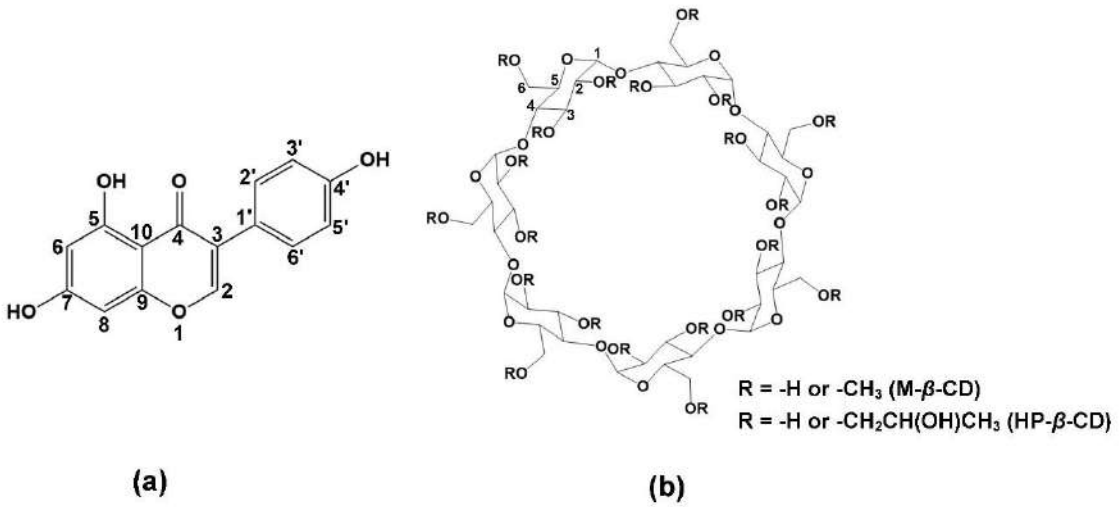

Figure 1: Schematic representation of chemical structures of (a) genistein (b) *β*-cyclodextrin, where R represents the substitution of –H or –CH3 in case of methyl-*β*-cyclodextrin (M-*β*-CD) and substitution of –H or -CH2CH(OH)CH3 in case of hydroxypropyl-*β*-cyclodextrin (HP-*β*-CD).

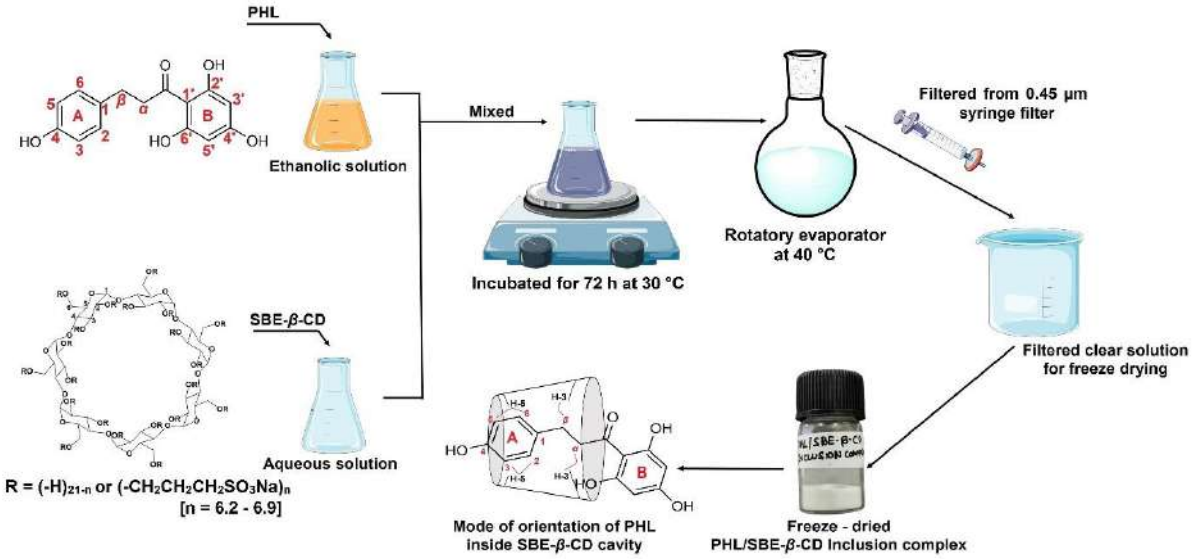

Figure 2: Schematic illustration of concept of study representing structure of phloretin and sulfobutylether-*β*-cyclodextrin, method of preparation of PHL/SBE-*β*-CD inclusion complex *via* lyophilization technique and mode of orientation of phloretin inside SBE-*β*-CD cavity (elucidated from 2D-NMR technique)

spectroscopy (^{1}H NMR & 2D NOESY). To gain deeper insights into the molecular interactions and binding dynamics, we employed classical molecular dynamics (MD) simulations and enhanced umbrella sampling simulations. These computational

approaches provided a detailed understanding of the conformational space and free energy landscapes of the inclusion complexes.

Furthermore, the in vitro dissolution profiles of the PHL/SBE-*β*-CD complex were evaluated, demonstrating significant improvements in solubility. The impact of the PHL/SBE-*β*-CD complex on cancer cell lines (A549 and MiaPaCa-2) was also assessed, revealing enhanced therapeutic efficacy through increased cell proliferation inhibition, caspase-3/7 activation, reactive oxygen species (ROS) generation, and mitochondrial membrane potential (MMP) depolarization.

Overall, this study highlights the potential of modified *β*-CDs, particularly SBE-*β*-CD, in enhancing the solubility and bioactivity of hydrophobic nutraceuticals like GEN and PHL, paving the way for their application in more effective therapeutic formulations.

2. Objectives:

- **Solubility and thermal stability enhancement:** The prime objective of this research work was development and optimization of inclusion complexes of genistein (GEN) and phloretin (PHL) with modified *β*-cyclodextrins (*β*-CDs) to significantly improve their aqueous solubility and thermal stability.
- **Characterization of inclusion complexes**: characterization of physical and chemical properties of the inclusion complexes of GEN with HP-*β*-CD and M-*β*-CD, and PHL with SBE-*β*-CD, using techniques such as FT-IR, Powder-XRD, SEM, TGA/DSC and NMR spectroscopy (^{1}H NMR & 2D NOESY).
- **Correlate experimental and computational findings**: correlate experimental observations with computational findings to provide a comprehensive understanding of the inclusion complexation process and its impact on the solubility, stability, and bioactivity of GEN.
- **Evaluate *In Vitro* dissolution profiles and therapeutic efficacy**: assess the *in vitro* dissolution profiles of the inclusion complexes, particularly focusing on the solubility enhancement of PHL when complexed with SBE-*β*-CD.
- **Examine therapeutic efficacy**: To evaluate the therapeutic potential of the PHL/SBE-*β*-CD inclusion complex in cancer treatment by investigating its effects on cell proliferation, caspase-3/7 activation, reactive oxygen species (ROS) generation, and mitochondrial membrane potential (MMP) depolarization in cancer cell lines (A549 and MiaPaCa-2).

- **Contribute to the field of cyclodextrin-based delivery systems**: To contribute new knowledge and insights into the field of cyclodextrin-based delivery systems, particularly focusing on the use of modified *β*-CDs to enhance the solubility and therapeutic efficacy of hydrophobic nutraceuticals.

3. Materials

Genistein ($C_{15}H_{10}O_5$, MW: 270.24 g/mol, >98 % Purity, Cas No. 446–72-0), *β*-cyclodextrin (MW: 1134.99 g/mol, >99.0 % Purity, Cas No. 7585–39-9), Phloretin ($C_{15}H_{14}O_5$, Mw: 274.27 g/mol, greater than 98.0 % Purity, Cas No. 60–82–2) was purchased from TCI chemicals. Methyl-*β*-cyclodextrin (Average Mn: 1310, Cas No: 128446–36-6), (2-Hydroxypropyl)-*β*-cyclodextrin (Average Mn: ~1460 g/mol, Cas No. 128446–35-5), Deuterium oxide (“100 %”, ≥ 99.96 atom % D, Cas No. 7789–20–0), DMSO-d_6 (“100 %”, ≥ 99.96 atom % D, contains 0.03 % (v/v) TMS, Cas No. 2206–27–1) were purchased from Sigma-Aldrich. Sulfobutylether-*β*-cyclodextrin (Captisol®, n = 6.3-6.9, Cas No. 182410–00-0) was offered as gift sample from CyDex Pharmaceuticals Inc. (Kansas, USA). Unless otherwise stated, analytical grades chemicals and reagents were used for experiments.

4. Methods

4.1. Quantitative analysis of PHL and GEN

The quantitative analysis of PHL was performed using Agilent HPLC (Agilent 1260 Infinity II, Waldbronn, Germany) equipped with quaternary pump (G7111A, 1260 Quat pump VL), an automatic vial sampler injector (G7129A, 1260 Vialsampler), a multicolumn thermostat (G7116A, 1260 MCT), and a DAD detector (G7115A, 1260 DADWR). The chromatographic separation was carried out using C18 reverse phase column (LiChrospher® 100 RP-18 Hibar® RT 250 mm × 4.6 mm, 5 µm, Darmstadt, Germany). The samples were eluted at a flow rate of 1 mL/min in isocratic mode using the mobile phase composed of [Eluent A: Acetonitrile; Eluent B: Water (0.01% TFA), (45:55 v/v)]. The detection of PHL was carried out at preset wavelength of 286 nm. The GEN was measured through HPLC (Waters 2000) equipped with empower

software utilized for data acquisition and analyzed on a pheominix 100-5 C18 column (250 × 4.6 mm, 5 µM) with isocratic elution (60:40 *v/v*) (Eluent A: Methanol; Eluent B: 0.1% Trifluoroacetic acid in water) with signal determination by PDA UV detector at 261 nm.

4.2. Determination of molar stoichiometry and apparent stability constant

Phase solubility studies were conducted accordingly as reported earlier with minor modifications. A surplus amount of flavonoid molecule was added in eppendorf tubes with 2 mL of *β*-CD derivatives (M-*β*-CD, HP-*β*-CD and SBE-*β*-CD) aqueous solution at various concentrations (0 to 10 mM), separately. The tubes were incubated in IKA® matrix orbital shaker (Delta F2.0, Germany) at 37°C with constant shaking for 48 h in dark and obtained suspension was filtered through 0.22 µm membrane filter. The Extent of solubility of flavonoid molecules were accessed by HPLC method discussed above. The phase solubility curves were plotted between the molar concentration of CDs and the molar concentration of GEN and the stability constant (Ks) was calculated from the slope of the plot as per Higuchi-Connor's equation:

$$Ks = \frac{Slope}{\mathrm{So}(1 - slope)}$$

Where S_o is the concentration of flavonoid molecules in absence of CDs and slope can be expressed from linear equation of phase solubility curves. The experiments are conducted in triplicates and results were expressed as mean ± SD (n=3).

4.3. Preparation of GEN: CD inclusion complexes (ICs)

The CDs that demonstrated the maximum solubility and apparent stability constant from phase solubility studies were chosen to prepare GEN ICs in a 1:1 molar stoichiometric ratio (GEN:CD). Briefly, GEN (5 mM, 0.27 g) solution was prepared in ethanol (40 mL) and M-*β*-CD (5 mM, 1.30 g) was dissolved in 160 mL of Milli-Q water. Similarly, the GEN-HP-*β*-CD ICs was prepared by dissolving HP-*β*-CD (5mM, 1.53 g) in MQ water, both the solution was mixed (GEN and CD solution) and placed over a magnetic stirrer for 24 hours. The obtained solution was fed for spray-drying in Buchi Mini Spray Dryer (B-290, Switzerland) with specified conditions of inlet temperature at 120°C ± 5°C and outlet temperature of 75 ± 5°C, respectively; feed rate of 4 mL/min;

aspiration rate of ~80%. Spray-dried GEN/CD powders were collected from the cyclone and stored in a tightly sealed container and kept in the refrigerator till further use.

4.4. Preparation of PHL/SBE-*β*-CD inclusion complex (IC)

On the basis of our phase solubility experiment, we have chosen SBE-*β*-CD as it demonstrated maximum solubility and apparent stability constant and PHL inclusion complex with SBE-*β*-CD was developed in a 1:1 molar stoichiometric ratio (PHL: SBE-*β*-CD). Briefly, PHL was dissolved in 12 mL ethanol (20 mM, 0.22 g) and SBE-*β*-CD (20 mM, 1.21 g) was dissolved in 28 mL of Milli-Q water. Both the solutions were mixed and incubated for 72 h at 30 °C on magnetic stirrer. Afterward, vaccum distillation at 40 °C using rotatory evaporator (IKA® RV 10) was carried out to remove the ethanol from the solution mixture. Then, to separate the undissolved PHL, the obtained solution was filtered through 0.45 µm syringe filter (Millipore Millex-HV, PVDF). Finally, the filtrate was collected and lyophilized by using freeze-dryer (Labonco, FreezeZone, Kansas City, MO, USA). The obtained PHL/SBE-*β*-CD-IC were stored in air-sealed container at cool place.

4.5. Preparation of the physical mixtures

The physical mixture was prepared for comparative study by the simple blending of GEN or PHL molecule with respective CD (1:1) for 15-20 min in a ceramic mortar pestle and obtained pulverized powders were sieved, stored in bottles and kept in the refrigerator.

5. Characterization of inclusion complexes (ICs)

5.1. Surface Morphology

The surface morphology of the specimens was visualized via scanning electron microscope (S-3400 N SEM, Hitachi, Tokyo, Japan). Prior to examination, a two-step sample preparation procedure was followed: firstly, the samples were spread over

brass stub with the aid of double-sided carbon adhesive tape. In the second step to avail the good electrical conductivity during microscopic scans, samples were coated with gold-palladium using ion sputter coater (Hitachi, E-1010) under an argon atmosphere. An accelerating voltage of 15 kV was used for carrying out imaging of the samples.

5.2. Fourier transform infrared spectroscopy (FT-IR)

The FT-IR spectrophotometer (PerkinElmer, USA, with software spectrum ES version 10.5.3) was used to acquire the FT-IR spectra of samples. The materials were mixed with potassium bromide (KBr) and then compressed using a hydraulic press to create KBr pellets. The spectrum was acquired with a resolution of 4 cm^{-1} in the spectral range of 4000 cm^{-1} and 400 cm^{-1}.

5.3. Recording of X-ray powder diffractometry (PXRD) pattern

The PXRD patterns of powdered samples were examined using smartLab 9 kW rotating anode X-ray diffractometer (Rigaku Corporation, Tokyo, Japan) equipped with a Cu-Kα radiation source. The instrumental analysis was performed at applied current of 40 mA and voltage of 40kV. The patterns were acquired as per mentioned parameters - diffraction angle (2θ); 5° to 60°, scan rate; 10°/min and step size; 0.2°.

5.4. Unveiling the mode of orientation through 1D and 2D – Nuclear magnetic resonance (NMR) spectroscopy analysis

^{1}H NMR spectra of the pristine flavonoid, cyclodextrin and inclusion complexes were obtained in order to better understand the intermolecular interaction between the host and guest molecules. The experimental parameters used to acquire the 2D-NOESY were 64 scans, 0.18 seconds for acquisition, and 2.0 seconds for relaxation. NMR spectra were recorded on 500 MHz NMR spectrometer (AV-500, Bruker, Switzerland),

at room temperature using D_2O/DMSO-d_6 (600 µL) as NMR solvent. The chemical shift was expressed in terms of parts per million (ppm) and changes in chemical shifts (∆δ) were calculated using following equation:

$$\boldsymbol{Chemical\ shift\ changes}\ (\Delta\boldsymbol{\delta}) = \boldsymbol{\delta}_{(complex)} - \boldsymbol{\delta}_{(free)}$$

5.5. Computational Datasets and modeling of Genistein Inclusion complexes (ICs)

The structures of GEN (CAS Number: 446-72-0), HP-*β*-CD (CAS Number: 128446-35-5) and M-*β*-CD (CAS Number: 128446-36-6), were downloaded in sdf format from the Pubchem database. The 2D structure files were converted to 3D format and subjected to geometry and energy minimization by Discovery Studio package (Studio, 2015). The CDOCKER protocol of Discovery Studio was utilized for modeling the GEN/HP-*β*-CD and GEN/M-*β*-CD ICs. CDOCKER produced 10 conformations each for both the complexes. The models with least interaction energy scores were selected for further investigations.

5.5.1. Molecular Dynamics (MD) simulations

The modeled GEN/HP-*β*-CD and GEN/M-*β*-CD ICs were selected as starting structures for MD simulation studies by GROMACS software. The MD simulations for both the complexes were carried out in different steps including topology generation, solvation, energy minimization, equilibration and finally subjected to MD production runs of 1000 ns (1 µs) each. The structural co-ordinates of GEN, HP-*β*-CD, and M-*β*-CD were extracted from the complex files and submitted to the PRODRG server for the generation of topologies compatible with GROMOS force fields (Schüttelkopf & Van Aalten, 2004). The GEN topologies were amended to HP-*β*-CD, and M-*β*-CD topologies and the resulting structures were placed inside a cubic simulation box filled with a simple point charge water model. In order to retain the electroneutrality of the system, Na^+ and Cl^- ions were added to the simulation box. In the next step, steric clashes or inappropriate geometry were removed by structure relaxation through energy minimization. The steepest descent minimization protocol with a maximum of 50000 steps and a maximum force cut-off value of <1000.0 kJ/mol/nm was used for energy minimization. The equilibration of the system was achieved in two steps under:

1000 ps NVT (particle number, volume, and temperature are kept constant) and 1000 ps NPT (particle number, pressure, and temperature are all constant) ensembles. The temperature of the system was maintained at 300K by V-rescale (modified Berendsen thermostat), while 1 bar reference pressure was maintained by the Parrinello-Rahman algorithm. The leap-frog integrator with a 2fs time step was used for the integration of the equations of motion. The SHAKE algorithm was employed for constraining bond lengths involving hydrogen atoms, while the long-range interactions were included by the Particle-Mesh Ewald (PME) method. The energy minimized and well-equilibrated structures were then allowed for production MD runs of 1000 ns. The built-in scripts of GROMACS software were used for the analysis of the resulting MD trajectories of both the complexes.

5.5.2. Umbrella Sampling Simulations

Umbrella sampling is a computational technique that improves the sampling of a system where ergodicity is obstructed by the form of the system's energy landscape. The structures corresponding to the least energy obtained from the analysis of Gibbs free energy landscape were subjected to umbrella sampling simulations. The umbrella sampling simulations were also carried out by the GROMACS package. First of all, a series of configurations along a reaction coordinate were generated by forcing the ligand molecule (GEN) to move out of the binding site along the unbinding pathway. A constant force of 250 kJ/mol/nm^2 was applied at a pull rate of 0.01 nm/ps through a virtual spring to simulate the unbinding of the ligand molecule. The configurations so obtained were scrutinized based on center of mass (CoM) distance for umbrella sampling windows, which were run in independent simulations. For the initial 3 nm CoM distance, the sampling windows were collected after every 0.15 nm, while a window spacing of 2.0 nm was selected for CoM distance greater than 3 nm. The dynamic sampling of spacing windows allowed enhanced details at lower CoM distances. A total of 80 sampling windows for both the complexes were generated and each configuration was independently subjected to 10 ns umbrella sampling simulations, resulting in a total of 800 ns simulation time. Finally, the Weighted Histogram Analysis Method (WHAM) was utilized to extract the potential of mean force (PMF) curves. The bootstrap method was used for error estimation and the binding energy (ΔG_{bind}) was calculated from the PMF curves of the complexes.

5.6. Determination of encapsulation efficiency, loading efficiency, thermal behavior, in-vitro dissolution and Anti-tumor activity of PHL/SBE-β-CD inclusion complex (IC)

5.6.1. Determination of embedding efficiency (EE) and loading efficiency (LE)

The percentage embedding efficiency (EE) and loading efficiency (LE) were determined as per previously reported method with appropriate modifications [22]. First, 10 mg of PHL/SBE-β-CD-IC was dissolved in 1 mL of milli-Q water and placed IKA® matrix orbital shaker for 48 h at 37°C. The obtained solution was centrifuged for 12,000 rpm for 15 min and supernatant was collected and filtered through syringe filter 0.45 µm (Millipore Millex-HV, PVDF) to remove the undissolved PHL. The PHL was quantified using HPLC system as per the method described in above section. The calculations have been performed using following equations:

$$EE\% = \frac{(Amount\ of\ PHL\ entrapped)}{(Initial\ amount\ of\ PHL\ added)} \times 100$$

$$LE\% = \frac{(Amount\ of\ PHL\ entrapped)}{(Amount\ of\ inclusion\ complex)} \times 100$$

5.6.2. Differential scanning calorimetry (DSC) analysis

The thermal behavior was analyzed using differential scanning calorimeter (DSC200, Hitachi). The DSC thermograms were acquired at a heating rate of 10 °C per minute and recorded in the range of 25 °C to 300 °C, under a dynamic nitrogen flow (50 mL/min). The samples were hermetically sealed in chromated aluminum pan containing approximately 3 – 5 mg of the samples and empty sealed chromated aluminum pan served as reference.

5.6.3. Thermal gravimetric analysis (TGA)

The thermal degradation curves of PHL, SBE-*β*-CD, PM and IC were analyzed using TGA/DSC thermal analyzer (Mettler Toledo, model: TGA/DSC-I, Columbus, OH, USA). The thermal degradation curves were acquired at heating rate of 10 °C/min over the temperature range from 25 °C to 700 °C, under dynamic nitrogen atmosphere.

5.6.4. In vitro dissolution test

The dissolution of pure PHL and PHL/SBE-*β*-CD-IC (equivalent to 20 mg PHL) was assessed using the USP apparatus II (*in vitro* dissolution apparatus, Lab India DS 8000) as per the procedure carried out by pal *et al.* with slight modifications. The experiment was carried out at physiological conditions: the dissolution chamber was filled with 900 mL of pH 7.2 phosphate buffer and was maintained 37 °C ± 0.05° C. The samples were filled in capsules and placed in dissolution chamber with aid of sinker. At specified time intervals (0, 30, 45, 60, 90 and 120 minutes), 5 mL of aliquots were withdrawn and to maintain the sink condition, subsequent replacement was done by adding 5 mL of freshly prepared dissolution media (pH 7.2 phosphate buffer) to the chamber. The collected sample aliquots were then filtered using membrane filter 0.45 µm syringe filter (Millipore Millex-HV, PVDF) and the filtrates were quantified for PHL content using HPLC system.

5.6.5. Cell culture and its maintenance

Human pancreatic cancer cell line (MiaPaCa–2) and lung carcinoma cell line (A549) were procured from the National centre for cell science (NCCS), Pune, INDIA. The cancer cell lines were grown in tissue culture flasks in complete DMEM, High glucose medium (Hi-Media) supplemented with 10% (v/v) fetal bovine serum (MP Biomedicals), 1X antibiotic- antimycotic (Gibco) in 5% CO_2 at 37°C in 95 % humidified

atmosphere. For cell viability assay, the cells were treated with various concentration (i.e., 10, 50, 100, 200 and 300 µM) of PHL and PHL/SBE-*β*-CD (equivalent to PHL amount) and for remaining experiments, cells were treated with PHL concentration (100, 150 and 200 µM) and PHL/SBE-*β*-CD (equivalent to PHL amount).

5.6.6. Cell viability assay by CCK-8 assay

The cytotoxicity of PHL, SBE-*β*-CD and PHL/SBE-*β*-CD-IC were evaluated in pancreatic cancer cells (MiaPaCa–2) and lung cancer cells (A549). The number of viable cells left after sample treatment was assessed by cell counting kit (CCK-8, Sigma-Aldrich). Briefly, both cells (MiaPaCa–2 & A549) were seeded at 5×10^3 cells per well in 96 well cell plate separately and incubated for 24 h at 37 °C. The cells were treated with PHL and PHL/SBE-*β*-CD-IC and further incubated for 24 h in CO_2 incubator. Following the incubation period, 10 µL of the CCK-8 reagent was added to each well and left to incubate for another 2 h at 37 °C. A microplate spectrophotometer (Infinite M200, TECAN) was used to determine the optical density at 450 nm.

The percentage cell viability at different concentration with respect to control (untreated cells) was calculated by using following equation:

$$\%\ Cell\ viability = \frac{OD\ test}{OD\ control} \times 100$$

5.6.7. Analysis of caspase 3/7 activation

To evaluate the apoptotic properties, apoptosis mediator (caspase3/7) activity was assessed using caspase-3/7 assay kit (CellEvent™ Caspase-3/7 Green Detection Reagent, Invitrogen by Thermo Fisher Scientific). The experiment was carried out as per the manufacturer's protocol. In brief, the MiaPaCa–2 and A549 cells were exposed to PHL or PHL/SBE-*β*-CD-IC for 24 h. Caspase reagent was diluted with 2 mL PBS

(1:400 ratio) before treatment in to the wells. In each well 5 µL of the diluted reagent was added, which was then incubated for 30 minutes at 37 °C. Finally, samples' GFP fluorescence was measured using an automated cell counter (Countess™ 3FL, Invitrogen, Thermo Fisher Scientific, Singapore) (λex = 502 nm, λem = 530 nm).

5.6.8. Estimation of ROS generation

The impact of ROS generation by PHL/SBE-*β*-CD-IC was assessed using fluorogenic cell permeant dye 2',7'-dichlorofluorescein diacetate (DCF-DA). For experiment, cell lines were seeded in 12-well microplates and incubated overnight at 37 °C. Thereafter, the cells were treated with PHL and PHL/ SBE-*β*-CD-IC for 24 h. After washing with PBS, the cells were exposed to 20 µM DCF-DA and incubated for 30 min at 37 °C . Prior to examination, the cells were re-washed with PBS and the fluorescence intensity was recorded using microplate spectrophotometer (Synergy-H1, hybrid reader, BioTek®) and imaging was performed at Ex-488 nm and Em-535 nm at x20 magnification using confocal microscope (Leica Stellaris 5, Illinois, USA).

5.6.9. Mitochondrial membrane potential (MMP) analysis

To evaluate the effect of PHL/SBE-*β*-CD-IC on the mitochondrial membrane potential, JC – 1 (Tetraethylbenzimidazolylcarbocyanine iodide, mitochondrial membrane potential probe, Invitrogen by Thermo Fisher Scientific) staining was carried out. In brief, MiaPaCa–2 and A549 cells were seeded for 24 h and after adherence, the cells were treated with various concentration of PHL and PHL/SBE-*β*-CD-IC for 24 h. Then after washing with PBS, JC-1 dye (2 µM) was added and left for 20 minutes in dark at 37 °C. At last, the final wash was given to remove the dye from the cells. The imaging was performed using confocal microscope (Leica Stellaris 5, Illinois, USA) at x20

magnification and by using ImageJ software (version,1.53e) the fluorescence intensity was determined.

6. Results and discussion

6.1. Determination of apparent stability constant (Ks) and molar stoichiometry

The phase solubility studies for PHL and GEN were conducted as a preliminary screening procedure to determine the molar stoichiometric ratios, stability constants (Ks), and solubilizing capabilities of various cyclodextrin (CD) derivatives. The studies revealed that both PHL and GEN formed inclusion complexes (ICs) with the CD derivatives, with the phase solubility curves of PHL/(2-HP)-*β*-CD, PHL/M-*β*-CD, PHL/SBE-*β*-CD, GEN/*β*-CD, GEN/M-*β*-CD, and GEN/HP-*β*-CD exhibiting linear increases in solubility with increasing CD concentration, indicating AL-type curves according to Higuchi and Connors. This linear relationship signifies a 1:1 molar stoichiometric ratio between the host (CD) and guest (PHL or GEN) molecules.

The apparent stability constants (Ks, M^{-1}) were calculated from the slopes of the linear phase solubility curves. For PHL, the stability constants were ranked as follows: SBE-*β*-CD (15,856 M^{-1}, strong binding) > M-*β*-CD (14,676 M^{-1}, strong binding) > (2-HP)-*β*-CD (11,452 M^{-1}, strong binding). In contrast, the stability constants for GEN were

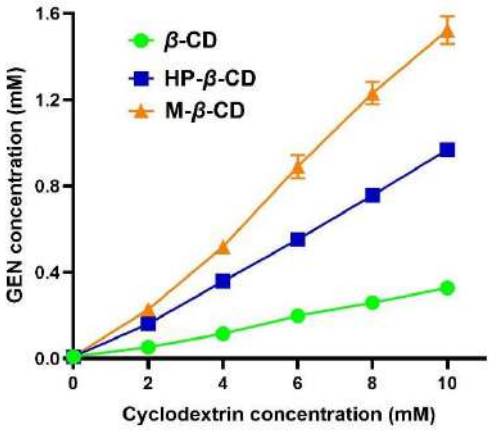

Figure 3: Phase solubility curve of genistein in aqueous solutions of *β*-cyclodextrin (green), M-*β*-CD (orange) and HP-*β*-CD (blue) with different concentrations (0-10 mM). The values were expressed as mean ± standard deviation (n=3).

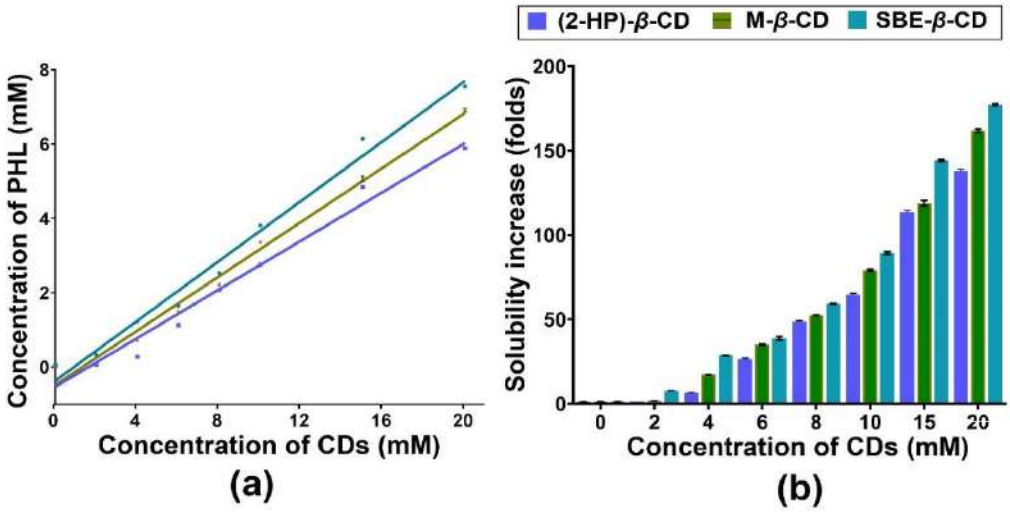

Figure 4: Determination of (a) Phase solubility curve of phloretin (PHL) at increasing concentrations of *β*-cyclodextrin derivatives (0-20 mM); (b) Folds increment in aqueous solubility of PHL in the presence of cyclodextrin (n=3)

ranked as: M-*β*-CD (20,005.98 M^{-1}, very strong binding) > HP-*β*-CD (11,587.10 M^{-1}, strong binding) > *β*-CD (3,662.58 M^{-1}, moderate binding) **(Figure 3).** According to the criteria set by Jacob et al., the binding affinities observed in this study indicate that both PHL and GEN exhibit strong to very strong binding with their respective CD derivatives.

The higher apparent stability constants for SBE-*β*-CD with PHL and M-*β*-CD with GEN suggest superior inclusion effects, potentially due to structural modifications in the CDs that enhance hydrogen bonding and expand the hydrophobic cavity. These modifications include the sulfobutyl moieties in SBE-*β*-CD, which provide increased negative charge and hydrophobic space, and the hydroxypropyl and methyl groups in M-*β*-CD, which contribute to enhanced binding affinities.

The solubility enhancements of PHL and GEN in the presence of these CDs were also significant. For PHL, SBE-*β*-CD increased solubility by ~177-fold, M-*β*-CD by ~161-fold, and (2-HP)-*β*-CD by ~138-fold at a 20 mM concentration compared to free PHL **(Figure 4).** Similarly, GEN solubility was enhanced by ~164-fold with M-*β*-CD and ~104-fold with HP-*β*-CD at a 10 mM concentration compared to free GEN. These results highlight the potential of SBE-*β*-CD for PHL and M-*β*-CD for GEN as ideal carriers for enhancing solubility and bioavailability.

6.2. Surface Morphology

A comparative analysis of the scanning electron microscopy (SEM) images provided morphological evidence of the successful formation of inclusion complexes (ICs) with both Genistein (GEN) and Phloretin (PHL) using different cyclodextrin (CD) derivatives.

The SEM micrograph of native GEN exhibited a well-defined crystal structure **(Figure 5 c).** In contrast, the surface morphology of M-*β*-CD and HP-*β*-CD revealed porous, spherical structures with variable cavity sizes and fragments, indicative of their amorphous nature. When examining the physical mixtures (PMs) of GEN with these CDs, the SEM images displayed a combination of distorted spherical particles and GEN crystals adhered to the surface of the CDs, suggesting limited interaction between the host and guest molecules. However, the SEM images of the spray-dried inclusion complexes of GEN with the CDs revealed significant changes in surface morphology, showing amorphous and homogeneous sphere-shaped structures with some uneven surfaces. These morphological changes indicate the presence of a new solid phase, effective encapsulation of GEN, and the efficiency of the spray-drying process.

Similarly, the SEM images of native PHL displayed rod-like crystal structures, whereas SBE-*β*-CD exhibited smooth, spherical shapes with cavity size variability and fragments **(Figure 6 a).** The SEM images of the physical mixture of PHL and SBE-*β*-CD showed distorted spherical particles of SBE-*β*-CD with PHL particles adhered to their surfaces, indicating minimal interaction between the molecules. In contrast, the freeze-dried inclusion complex of PHL with SBE-*β*-CD demonstrated a smooth surface with the complete disappearance of the distinctive rod-like crystals of PHL (Figure 2(c)). These observations suggest that the formation of the PHL/SBE-*β*-CD inclusion complex resulted in significant surface morphological changes, indicating successful formation of a new solid phase, efficient incorporation of PHL within the CD cavity, and the effectiveness of the lyophilization process.

Overall, the SEM analysis provided clear morphological evidence of the successful formation of inclusion complexes in both studies, with significant alterations in the native morphologies of the guest molecules (GEN and PHL) and the CD carriers.

These changes are indicative of effective encapsulation and the creation of new solid phases, affirming the efficiency of the spray-drying and lyophilization methods used in the preparation of the inclusion complexes.

6.3. Fourier-transform infrared spectroscopy (FT-IR) analysis

FT-IR spectroscopy was employed to investigate the potential interactions between the functional groups of the guest molecules (Genistein [GEN] and Phloretin [PHL]) and the host cyclodextrin (CD) derivatives (M-*β*-CD, HP-*β*-CD, and SBE-*β*-CD). The formation of inclusion complexes (ICs) is typically characterized by alterations in peak intensity, broadening, shifting, and even disappearance in the FT-IR spectra, indicating the molecular interactions between the host and guest molecules.

The FT-IR spectra of GEN, its CD derivatives (M-*β*-CD, HP-*β*-CD), their physical mixtures (PMs), and the inclusion complexes (ICs) are presented in **(Figure 5 a).** GEN displayed characteristic peaks at 3410 cm^{-1} (O-H stretching) and 3088 cm^{-1} (aromatic C-H stretching), along with other significant peaks at 1652 cm^{-1} (C=O stretching), 1615 cm^{-1} (C=C stretching), 1320-1150 cm^{-1} (C-O-C stretching), and 1260-1000 cm^{-1} (C-O stretching). The spectra of M-*β*-CD and HP-*β*-CD showed prominent O-H stretching vibrations at 3415.32 cm^{-1} and 3409.41 cm^{-1}, respectively, alongside other characteristic peaks corresponding to C-H and C-O stretching vibrations.

In the physical mixtures (PMs), the characteristic peaks of GEN and CDs were mostly superimposed, indicating minimal interaction between the host and guest molecules. However, in the spectra of the inclusion complexes, several of GEN's characteristic absorption bands, particularly the O-H stretching peak at 3410 cm^{-1}, were either reduced in intensity or completely concealed by the broad bands of the CDs. This suggests that the O-H groups of GEN likely participated in hydrogen bonding with the CD molecules, leading to the formation of ICs. Additionally, the absence or reduction of certain GEN peaks (1500-1000 cm^{-1} and 3000-2000 cm^{-1} regions) in the IC spectra further supports the successful inclusion of GEN within the CD cavities.

Similarly, the FT-IR spectra of PHL, SBE-*β*-CD, their physical mixture, and the resulting IC are depicted in **(Figure 6 b).** PHL exhibited a broad absorption band ranging from 3351.11 to 3189.62 cm^{-1}, attributed to O-H stretching vibrations, alongside prominent bands at 1607.02 cm^{-1}, 1571.79 cm^{-1}, and 1513.06 cm^{-1} corresponding to the stretching vibrations of the C=C bonds in the aromatic ring. The

SBE-*β*-CD spectrum displayed a broad O-H stretching band from 3762.23 to 3104.47 cm^{-1}, with additional bands corresponding to C-H stretching and O=S=O group vibrations.

In the physical mixture, the spectra were a simple superimposition of PHL and SBE-*β*-CD, with no significant changes observed. However, in the IC spectra, the broad absorption bands of the hydroxyl groups and asymmetrical stretching vibrations of the $-CH_2$ groups exhibited noticeable changes in intensity and width compared to the PM and pure molecules. Furthermore, several characteristic peaks of PHL were masked, shifted, or reduced in the IC spectra, indicating the potential embedding of PHL inside the SBE-*β*-CD cavity. These spectral discrepancies between the free and complexed forms of PHL strongly suggest successful IC formation.

The clear differences in the FT-IR spectra between the free guest molecules (GEN and PHL) and their respective ICs with the CDs provide compelling evidence of molecular interactions and successful inclusion complexation. Nevertheless, additional characterization techniques were employed to further confirm the formation and stability of these ICs.

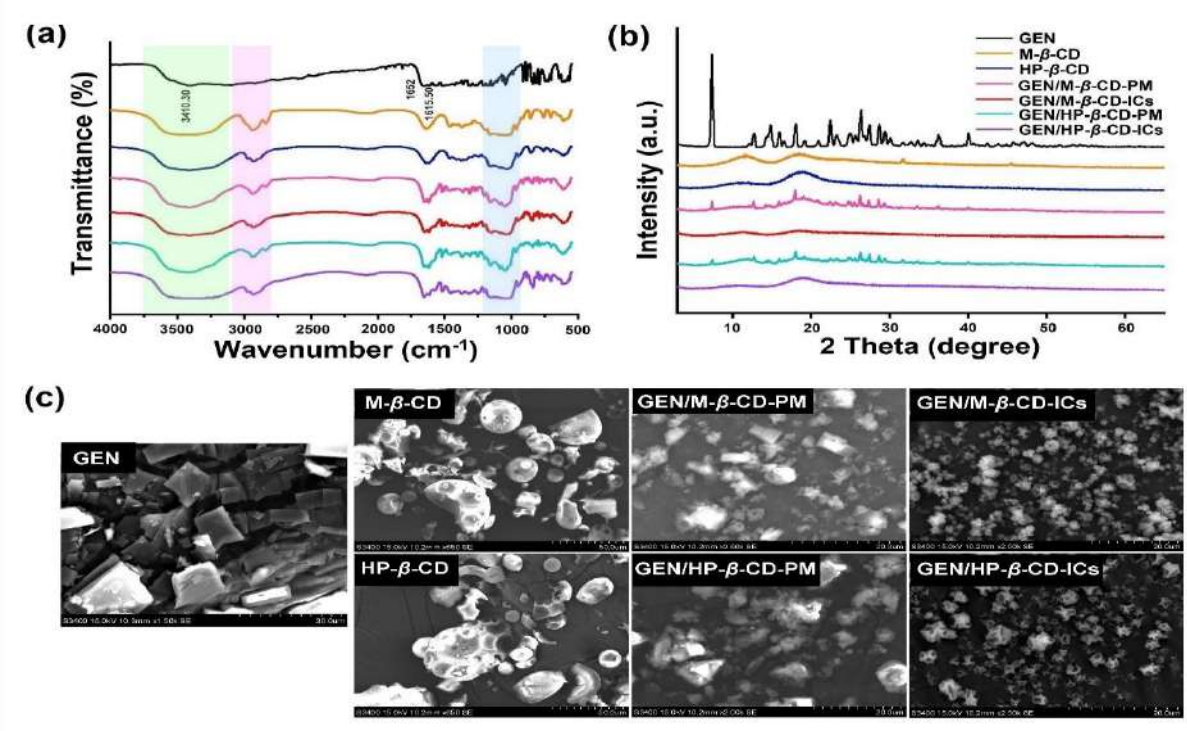

Figure 5: Solid state characterization of developed inclusion complexes (ICs) using (a) FTIR, (b) PXRD spectra and (c) SEM. The FTIR spectra, green, pink and blue regions indicate shifted, decreased and concealed characteristic absorption peaks of genistein after inclusion complex formation

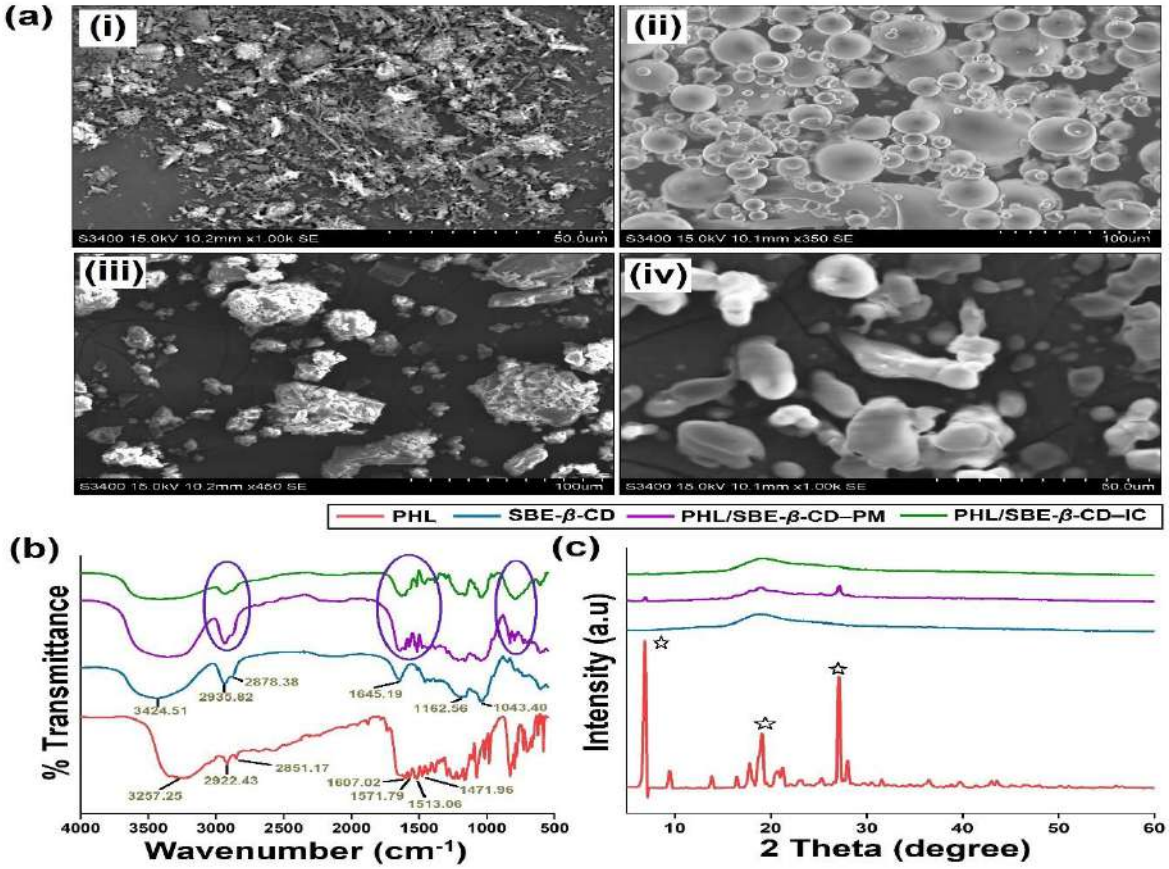

Figure 6: (a) Scanning electron microscopy of (i) PHL, (ii) SBE-*β*-CD, (iii) PHL/SBE-*β*-CD inclusion complex and (iv) corresponding physical mixtures; (b) Stacked FT-IR spectra and (c) PXRD diffractograms of PHL, SBE-*β*-CD, PHL/SBE-*β*-CD inclusion complex and corresponding physical mixtures. In FTIR spectra, oval marking indicates shifted, decreased, and concealed prominent absorption peaks and bands of PHL after formation of inclusion complex. In XRD diffractograms of PHL, star indicates its intensive sharp crystalline peaks at 2θ degree: 6.94°, 19.1° and 27.12°.

6.4. Powder X-ray diffractometry (PXRD) analysis

PXRD is a robust analytical technique for characterizing the crystalline or amorphous nature of inclusion complexes (ICs). The PXRD patterns of native Genistein (GEN) revealed several sharp peaks at diffraction angles 7.38°, 12.74°, 14.44°, 14.82°, 15.94°, 18.04°, 22.44°, 23.16°, 23.34°, 24.92°, 25.06°, 26.38°, 27.40°, 28.68°, and 40.0°, indicating its crystalline structure **(Figure 5 b).** In contrast, the PXRD patterns of M-*β*-CD and HP-*β*-CD exhibited smooth curves without any crystalline peaks, reflecting their amorphous nature. When examining the physical mixtures (PMs) of GEN with these CDs, the diffractograms showed combined characteristic patterns of GEN with their respective CDs, with significantly weakened peaks of GEN compared to pure GEN. However, the PXRD spectra of the GEN-CD inclusion complexes

displayed an amorphous pattern similar to their parent CDs, with a complete disappearance of the crystallization peaks of GEN. This transition from a crystalline to an amorphous form indicates that the GEN molecules were successfully encapsulated within the CD cavities during the IC formation process, thereby preventing the aggregation of GEN molecules to form crystals.

Similarly, the PXRD analysis of native Phloretin (PHL) displayed distinct sharp peaks at diffraction angles 6.94°, 19.1°, and 27.12°, along with several minor peaks on the 2θ scale, confirming its crystalline nature **(Figure 6 c)**. In contrast, the diffractogram of SBE-*β*-CD did not exhibit any prominent peaks, instead showing a hollow, amorphous pattern consistent with its amorphous nature. The PXRD pattern of the physical mixture of PHL with SBE-*β*-CD was essentially a summation of the individual diffractograms, with diminished peaks of PHL at 6.94° and 27.12°, indicating limited interaction between the molecules. However, the PXRD pattern of the PHL-SBE-*β*-CD inclusion complex displayed a completely amorphous hollow pattern, similar to that of SBE-*β*-CD, with comprehensive masking of the crystalline peaks of PHL. This result suggests that during the lyophilization process, PHL was effectively encapsulated within the SBE-*β*-CD cavity, thereby preventing the molecular aggregation of PHL and resulting in the transformation of PHL from a crystalline state to an amorphous form.

6.5. Proton nuclear magnetic resonance (^{1}H NMR) and two–dimensional nuclear overhauser effect spectroscopy (2D – NMR)

NMR spectroscopy is a reliable method for analyzing supramolecular interactions within host-guest assemblies, providing molecular-level insights into inclusion complex (IC) formation. The interactions between the host (cyclodextrins) and guest molecules (Genistein [GEN] and Phloretin [PHL]) cause chemical shift differences (Δδ) in the NMR spectrum due to changes in the chemical and electronic environments of the involved nuclei.

For Phloretin (PHL), the ^{1}H NMR spectra revealed characteristic peaks at ~12.18 ppm, 10.28 ppm, and ~9.07 ppm, corresponding to the hydroxyl groups of H-6'-OH, H-2'-OH, H-4'-OH, and H-4-OH, respectively. Additionally, peaks at 7.02 ppm, 6.67 ppm, 5.81 ppm, 3.22 ppm, and 2.78 ppm were observed due to H-2,6, H-3,5, H-3',5', H-*β*,

and H-α, respectively. The chemical shifts of SBE-*β*-CD were observed between 1.5

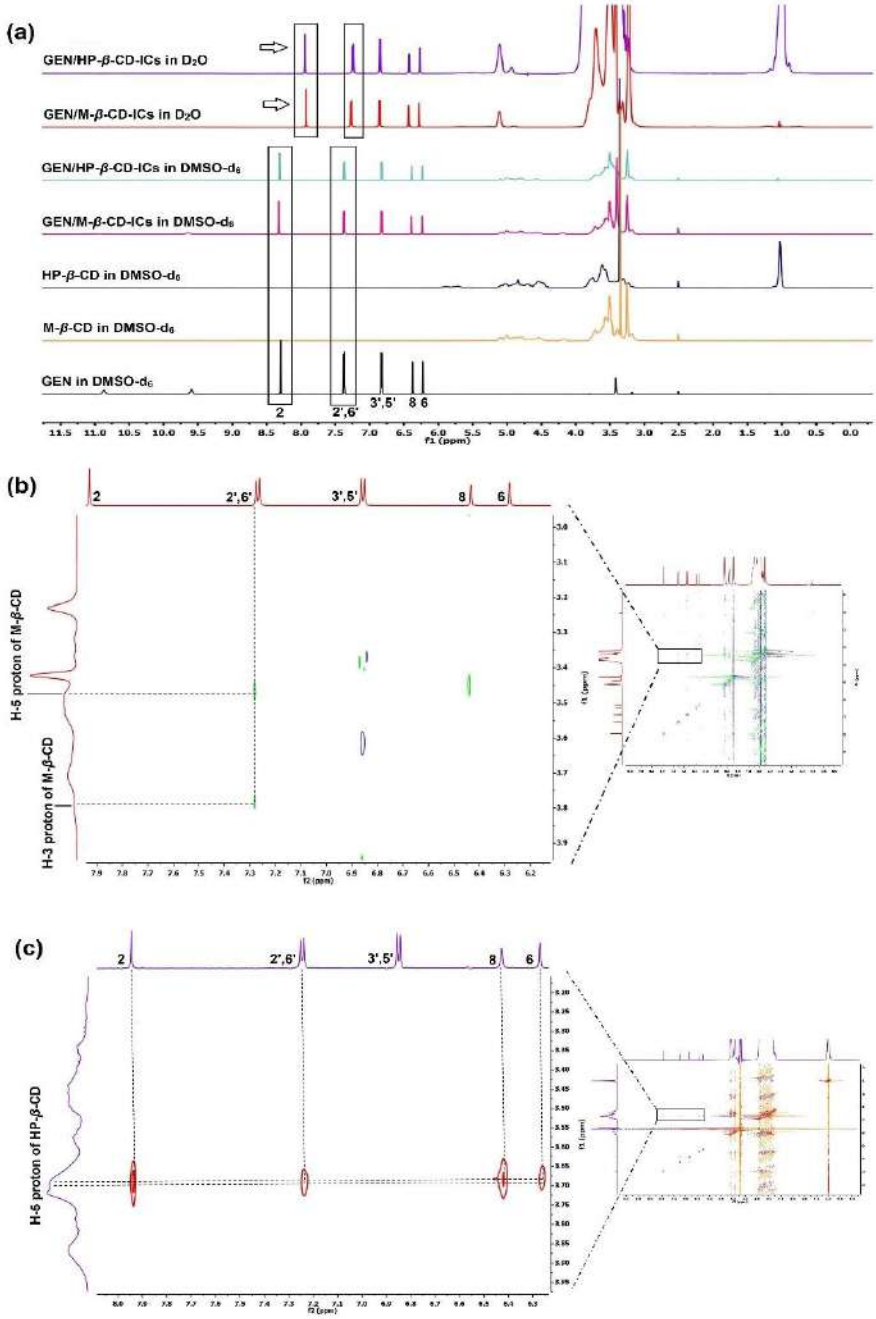

Figure 7: Nuclear magnetic resonance spectroscopy characterization of inclusion complexes (ICs) (a) ^{1}H NMR of GEN, M-*β*-CD, HP-*β*-CD and their ICs in DMSO-d_6 & D_2O and (b) 2D-NOESY spectra of GEN/M-*β*-CD-ICs and (c) GEN/HP-*β*-CD-ICs in D_2O. The chemical shift at 4.79 ppm and 2.50 ppm was observed due to D_2O & DMSO-d_6.

δ and 5.3 ppm, with specific δH values at 5.24 ppm, 3.62 ppm, 5.11 ppm, 3.50 ppm, 3.89 ppm, and 3.73 ppm for H-1, H-2, H-3, H-4, H-5, and H-6 protons, respectively. Upon forming the PHL/SBE-*β*-CD inclusion complex, significant downfield shifts were

noted, particularly for the H-2,6 and H-3,5 protons of the aromatic phenyl ring of PHL (Δδ of -0.053 ppm and -0.149 ppm, respectively). This indicated the successful inclusion of PHL within the SBE-*β*-CD cavity, as evidenced by the disappearance of proton signals for H-α and H-*β* due to overlapping with SBE-*β*-CD protons **(Figure 8).**

Similarly, the ^{1}H NMR spectra of Genistein (GEN) depicted peaks at ~12.97 ppm, ~10.86 ppm, and ~9.58 ppm for the -OH groups of H-5-OH, H-7-OH, and H-4'-OH, respectively. Additional peaks at ~8.30 ppm, ~7.37 ppm, ~6.83 ppm, ~6.37 ppm, and ~6.22 ppm corresponded to H-2, H-2',6', H-3',5', H-8, and H-6, respectively. The chemical shifts of HP-*β*-CD and M-*β*-CD were consistent with previously reported values, with characteristic peaks in the range of ~4.83 ppm to ~1.02 ppm for HP-*β*-CD and ~4.91 ppm to ~3.25 ppm for M-*β*-CD. The ^{1}H NMR spectra of the GEN-CD inclusion complexes exhibited significant chemical shift differences, with H-2, H-2', and

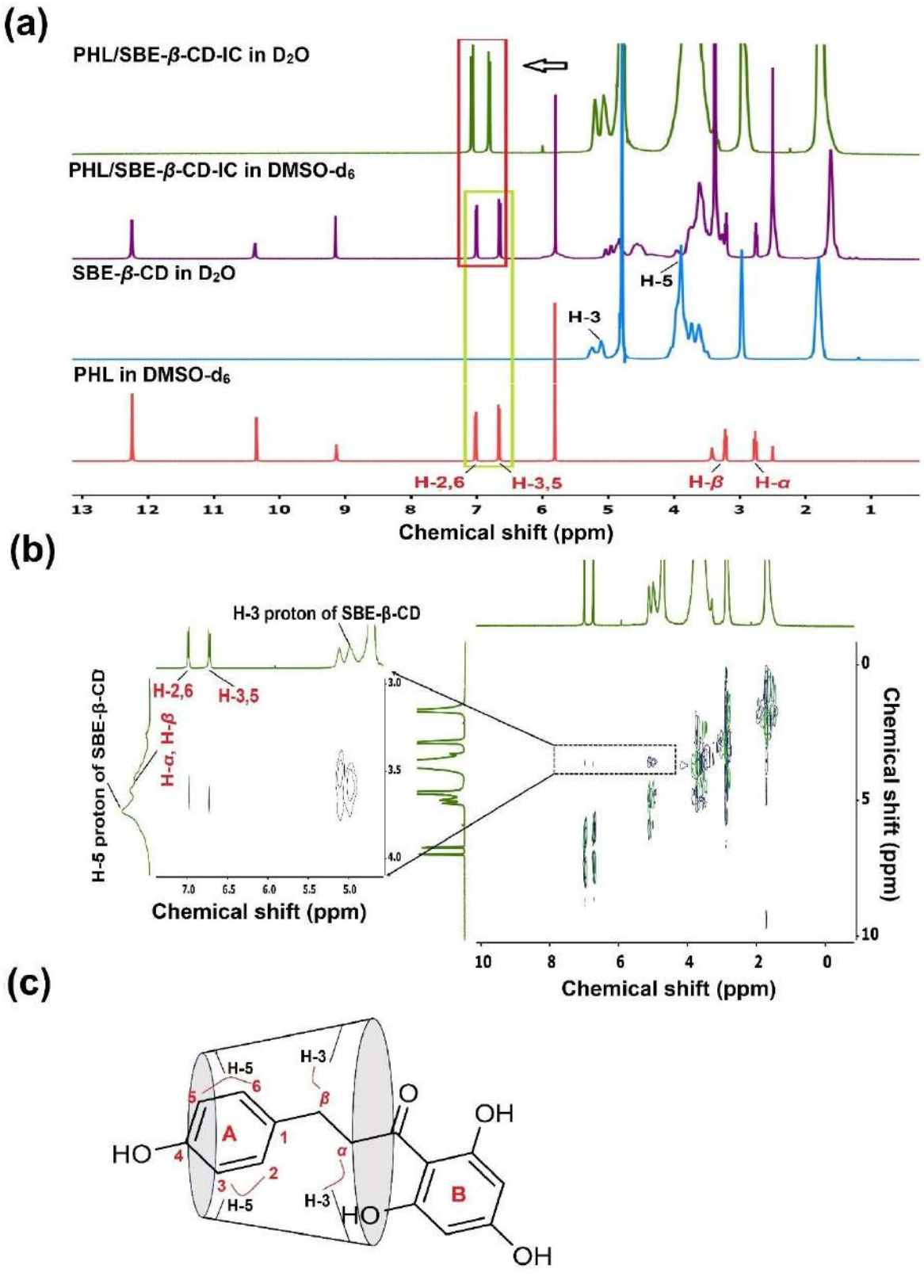

Figure 8: Unveiling the mode of orientation PHL inside the SBE-*β*-CD portal via nuclear magnetic resonance spectroscopy (a) 1H-NMR of PHL (in DMSO-d6), SBE-*β*-CD (in D2O) and PHL/SBE-*β*-CD (in DMSO-d6 and D2O); (b) 2D-NOESY spectra of PHL/SBE-*β*-CD-IC in D2O. The chemical shift at 4.79 ppm and 2.50 ppm was observed due to D2O and DMSO-d6, respectively. (c) Schematic

representation of mode of orientation of PHL inside SBE-*β*-CD cavity demonstrating protons of PHL interacting with protons lying in the inner cavity of cyclodextrin.H-6' protons of GEN showing upfield shifts (Δδ of -0.370 ppm, -0.100 ppm, and -0.100 ppm, respectively) in the GEN-M-*β*-CD ICs. Similarly, slight downfield shifts were observed for H-6, H-8, H-3', and H-5' protons.

To further elucidate the mode of inclusion, 2D-NOESY analysis was performed for both PHL/SBE-*β*-CD and GEN/CD inclusion complexes. For PHL/SBE-*β*-CD, the 2D-NOESY spectra demonstrated key correlations between the H-5 protons of SBE-*β*-CD and the aromatic doublets (H-2,6 and H-3,5) of the hydroxyphenyl moiety (ring-A) of PHL, leading to significant downfield shifts in the protons within the SBE-*β*-CD cavity (H-5 and H-3 protons). These findings suggest that the aromatic hydroxyphenyl ring (ring A) of PHL was inserted into the SBE-*β*-CD cavity from the wider side of the rim **(Figure 8)**.

Similarly, the 2D-NOESY spectra of GEN/M-*β*-CD ICs revealed correlations between the aromatic doublets of GEN's 4-hydroxyphenyl moiety with the H-3 and H-5 protons of M-*β*-CD, inducing chemical shifts in these protons. In contrast, the 2D-NOESY spectra of GEN/HP-*β*-CD ICs demonstrated cross-correlation peaks between GEN's H-2, H-2',6', H-8, and H-6 protons with the H-5 protons of HP-*β*-CD, causing downfield shifts. This indicates that the phenyl ring of GEN is inserted into the M-*β*-CD cavity from the wider side of the rim, whereas the chromone ring of GEN enters the HP-*β*-CD cavity from the wider rim edge **(Figure 7).**

These NMR findings collectively confirm the successful formation of inclusion complexes in both studies, corroborating the evidence obtained from other solid-state characterization techniques such as FTIR, PXRD, and DSC.

6.6. Conformational stability of selected GEN-ICs

MD simulation methods are often described as computational molecular microscopes for their ability to decipher the structure and behavior of various molecules, complexes, and mixtures on a molecular level. The root-mean-square deviations (RMSD) of backbone Cα atoms has been widely used for analyzing the stability of modeled CD complexes. The conformational stability of the modeled GEN/HP-*β*-CD and GEN/M-*β*-CD ICs was accessed by calculating the RMSD for the whole simulation run (**Figure 9a**). The stability of a complex is inversely related to the number of deviations occur during the simulations. We observed no major deviations in the RMSD values for both

the complexes. Although the overall trajectory was stable, minor deviations at two different time intervals (~300-500 ns and ~700-750 ns) were observed for GEN/M-*β*-CD complex. These deviations suggested multiple stable conformations achieved by GEN/M-*β*-CD complex during the simulations. The average RMSD values for GEN/HP-*β*-CD and GEN/M-*β*-CD ICs were 0.416 nm and 0.417 nm respectively. The low deviations and stable trajectories for both the complexes suggested high equilibration and conformational stability during the simulations.

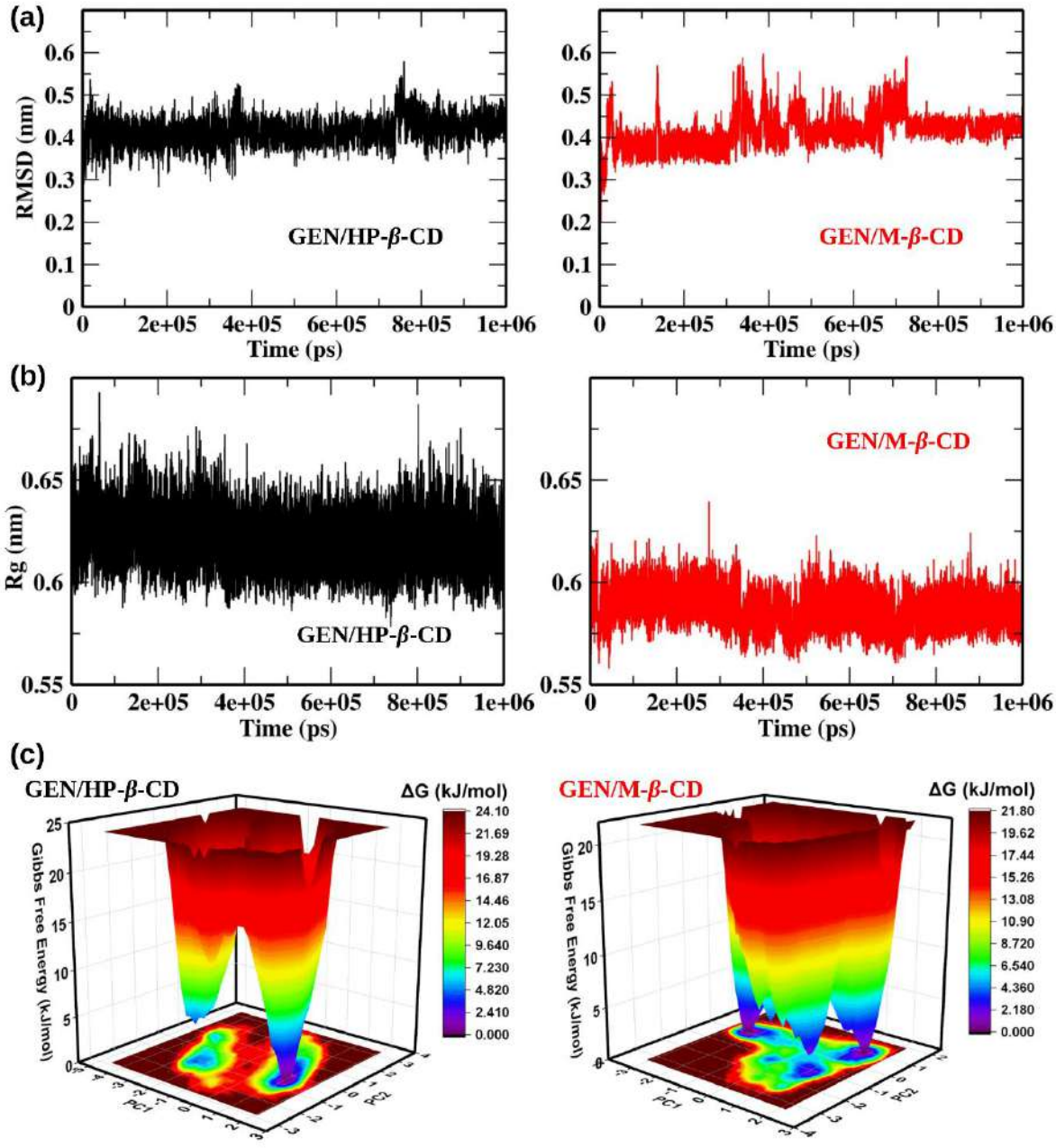

Figure 9: Assessing stability of modelled GEN/*β*-CD derivatives inclusion complexes (ICs) by classical MD simulations. (a) Root mean square deviations (RMSD) of backbone C*α* atoms of GEN/HP-*β*-CD

and GEN/M-*β*-CD ICs (b) Radius of gyration for GEN/HP-*β*-CD and GEN/M-*β*-CD ICs, and (c) Gibbs free energy landscape (FEL) showing local minimas for GEN/HP-*β*-CD and GEN/M-*β*-CD ICs.

6.7. Compactness of structures

In order to compare the encapsulation process of GEN into HP-*β*-CD and M-*β*-CD during MD simulations, the compactness and packaging of both the ICs were determined by accessing their Radius of gyration (Rg) (**Figure. 9 (b)**). Rg illustrates the mass-weighted root mean square distance from the center of mass of atoms under investigation. Several computational studies have utilized Rg for the estimation of the compactness of protein, protein-ligand, and CD-IC structures. The Rg values for GEN/HP-*β*-CD and GEN/M-*β*-CD structures were 0.61 nm and 0.68 nm, respectively. The Rg curves showed that GEN/M-*β*-CD had lower Rg values than GEN/HP-*β*-CD throughout the simulations. Lower Rg values indicate higher compactness and tighter packaging of GEN/M-*β*-CD than GEN/HP-*β*-CD. These results also resonate with experimental solubility studies, where GEN was shown to be more soluble in M-*β*-CD than HP-*β*-CD.

6.8. Gibbs free energy landscape (FEL)

The FEL reflects the kinetics and thermodynamics of any molecular processes in solution. The FELs are generally analyzed for the detection of the most stable conformations achieved by a given system during MD simulations. The Gibbs FELs were plotted for GEN/HP-*β*-CD and GEN/M-*β*-CD ICs from the MD trajectories by Boltzmann inverting multi-dimensional histograms method **(Figure. 9 (c))**. In order to explore the conformational shifts during the binding process of GEN with substituted *β*-CDs, the Gibbs FEL for the first two principal components (PC1 and PC2) was calculated. The first two PCs are usually the most vital among all the PCs to analyze the changes in Cα displacements during MD simulations. The metastable conformation achieved by structures are shown by the deep low free energy valleys, while the shallow basins depict energetic barriers connecting these states. The GEN/HP-*β*-CD IC showed a single deep valley achieving the least value of free energy. In the case of modeled GEN/M-*β*-CD structure, we observed two distinct energy minimas which correspond to metastable conformations. These results are consistent with the RMSD analysis, where GEN/HP-*β*-CD showed deviations at two distinct time intervals. Further, we investigated different binding poses opted by GEN and both the

modified *β*-CDs by extracting the trajectories of both the complexes at different time intervals.

6.9. Binding poses at different time intervals

Biological processes and structures related to receptor-ligand binding adopt multiple conformations that are linked to their biological functions. The experimental methods including NMR, X-ray crystallography, or electron microscopy can illustrate some of the structural heterogeneity, but are unable to demonstrate the detailed conformational transitions and dynamics. The analysis of intermolecular interactions at different time intervals extracted from the MD trajectories can provide a comprehensive analysis of the receptor-ligand binding dynamics **(Figure 10)**. In the case of GEN/HP-*β*-CD IC, initially (at 0 ns), GEN interacted with the hydrophilic surface of the HP-*β*-CD molecule. Thereafter, the chromone ring of GEN entered into the cavity of HP-*β*-CD and remained inside the hydrophobic core till ~800 ns. We observed a change in the binding orientation of GEN at 800 ns which reverted to its stable form at the end of the simulation. These results are consistent with our RMSD analysis where a slight deviation was observed around 800 ns (refer to Figure 9 a). Interestingly, in the case of GEN/M-*β*-CD IC, GEN showed two orientations inside the hydrophobic core of M-*β*-CD. The phenyl ring occupied the central cavity of M-*β*-CD at 0 ns, followed by a shift in orientation at 200 ns, resulting in an IC where the chromone ring occupied the cavity of M-*β*-CD. Afterward, the phenyl ring reoccupied the central cavity at 600 ns, again followed by a conformation shift that led the chromone ring inside the hydrophobic core of M-*β*-CD. These results are in perfect sync with our analysis of FEL where we observed two stable conformational states approaching the least energy values (refer to Figure 9 c). The possibility of two orientations of GEN inside the central cavity of unsubstituted *β*-CD was also explored in a previous study. The strength of interactions between GEN and the substituted forms of *β*-CD was further analyzed by calculating the free energy through enhanced sampling simulations.

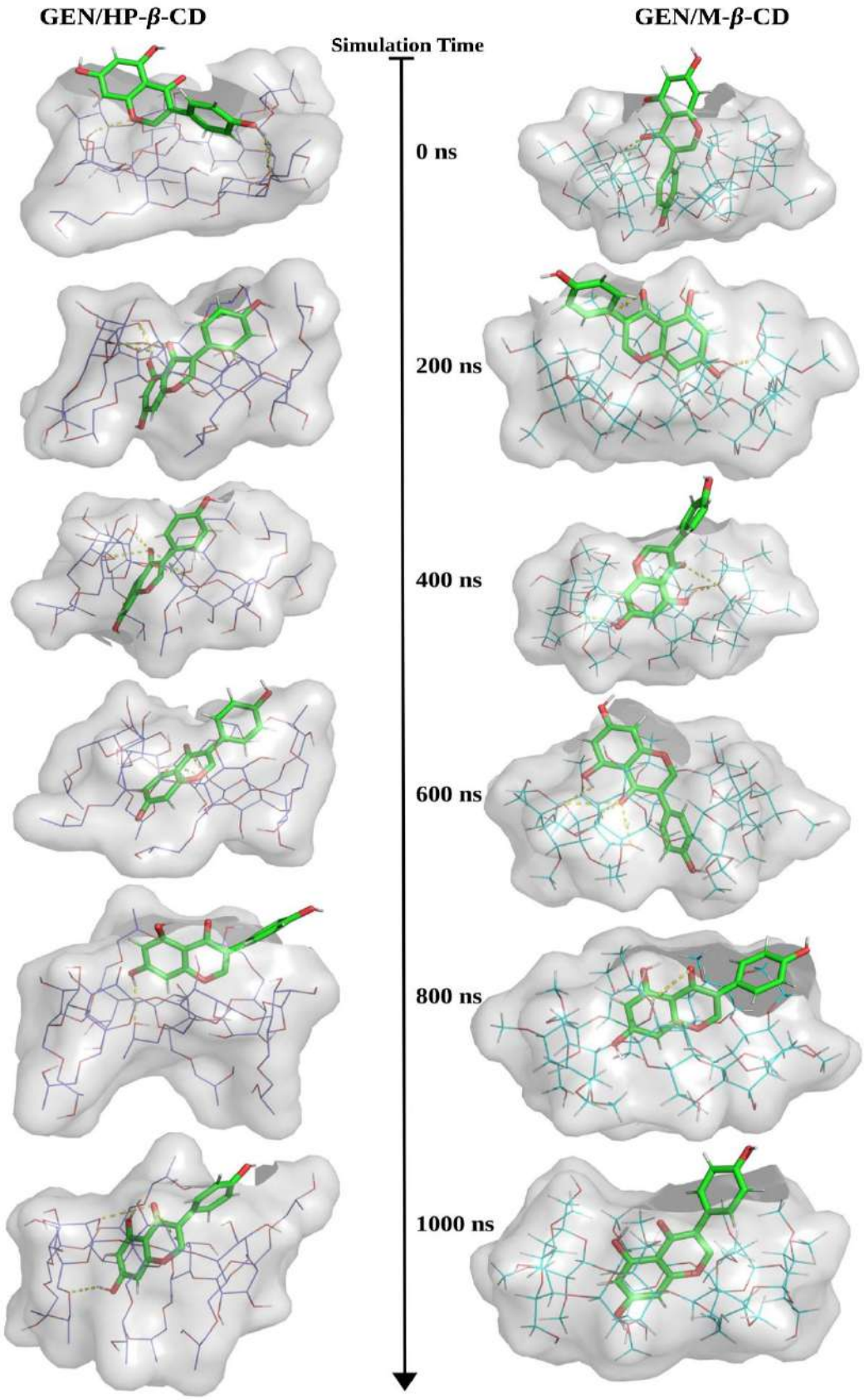

Figure 10: Analysis of conformational changes in GEN binding with HP-*β*-CD (left) and M-*β*-CD (right) at different time intervals (0, 200, 400, 600, 800, and 1000 ns) during MD simulations.

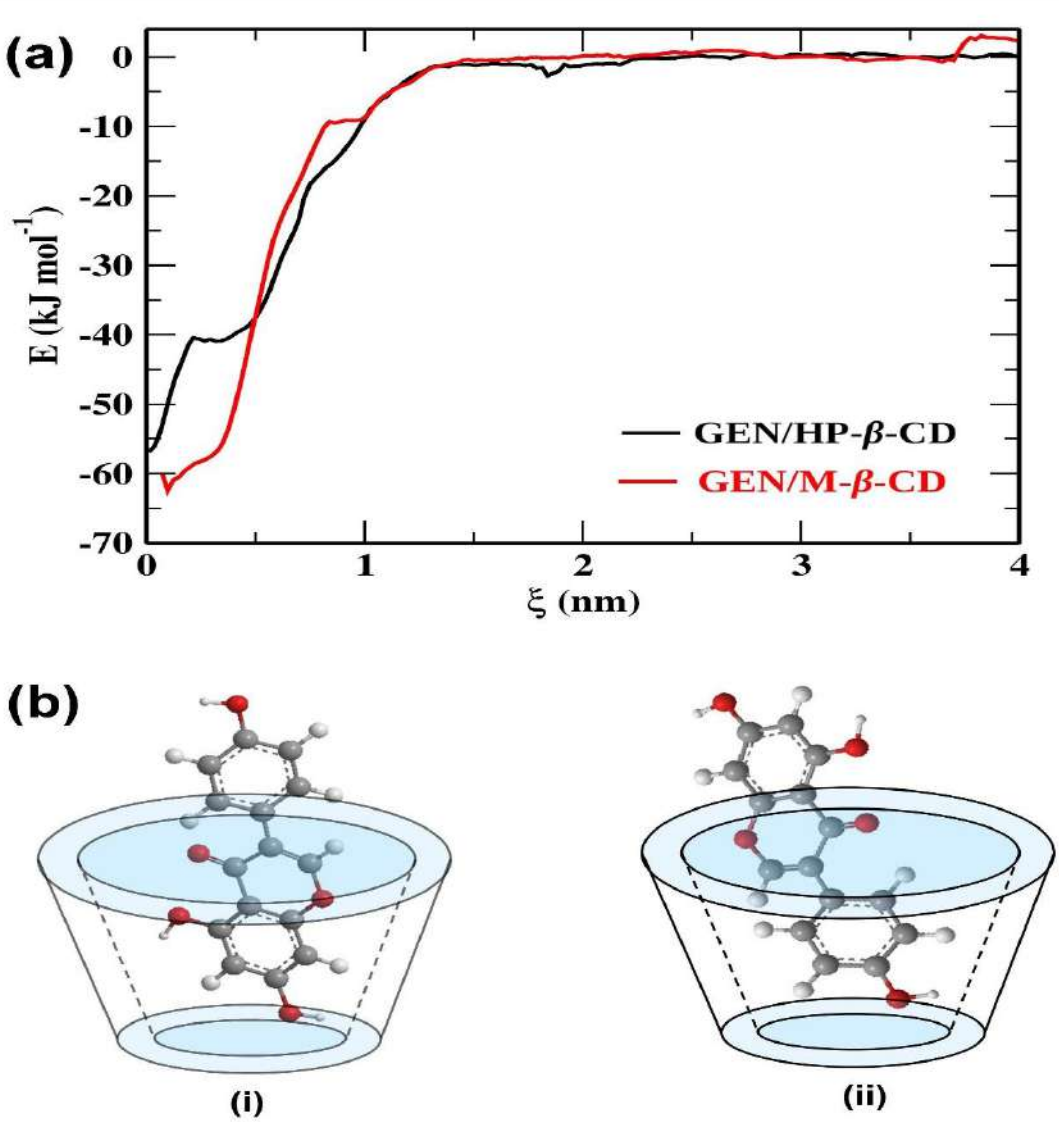

Figure 11: Potential of mean force (PMF) curves and mode of orientations of GEN inside the cavity of cyclodextrins. (a) A plot showing the potential of mean force (PMF) curves obtained from enhanced umbrella sampling simulations for GEN/HP-*β*-CD and GEN/M-*β*-CD complexes and (b) two different modes of orientations of GEN inside the cavity of cyclodextrins, where in case of HP-*β*-CD (i) orientation was found to be most stable one after MD simulations whereas, in case of M-*β*-CD both (i and ii) the orientations were found to be stable.

6.10. Umbrella sampling simulations

The directionality and the magnitude of binding/unbinding kinetics are governed by the change in the free energy of a system. The estimation of the free energy profile of a chemical or biological process is a challenging process in biochemistry and computational biology. Umbrella sampling, also referred to as biased MD simulations is a well-established technique to estimate free energy along a reaction coordinate of

non-covalent receptor-ligand systems including large biological systems and small chemical molecular systems. The distance between the modified *β*-CDs and GEN was calculated and selected to represent the reaction coordinate (ξ). The distance was recorded by employing steered MD simulations. The GEN molecule was allowed to move out of the binding site along the z-axis from the HP-*β*-CD and M-*β*-CD ICs. A total of 80 sampling windows along the reaction coordinate for both the complexes were subjected to independent biased MD simulations. The weighted histogram analysis method (WHAM) was employed for removing the biasing potential and construction of the potential of mean force (PMF) curves. The GEN/M-*β*-CD complex achieved the lowest energy value of -62.44 kJ/mol at 0.098 nm, while for the GEN/HP-*β*-CD structure, the minimum energy was -56.87 kJ/mol **(Figure 11).** The PMF curves were further exploited to extract the change in energy (ΔG) for both the complexes. The ΔG values for HP-*β*-CD and M-*β*-CD ICs were -57.76 kJ/mol and -65.58 kJ/mol respectively. These results indicated that GEN demonstrated stronger interactions with M-*β*-CD than HP-*β*-CD structures.

6.11. Determination of encapsulation efficiency, loading efficiency, thermal behavior, in-vitro dissolution and Anti-tumor activity of PHL/SBE-β-CD inclusion complex (IC)

6.11.1. Determination of embedding and loading efficiency

The embedding efficiency directly represents the capability of cyclodextrin to encapsulate the guest molecule. The PHL/SBE-*β*-CD-IC displayed embedding efficiency of ~ 69.13 ± 0.93% indicating significant potential of SBE-*β*-CD to encapsulate the PHL. The loading content was observed to be 8.57 ± 0.12% revealing exceptional quality of prepared IC to load the PHL molecule.

6.11.2. Differential scanning calorimetry (DSC)

The DSC curve of PHL demonstrated a sharp endothermic peak at 269.12 °C, implying the melting point (T_m) of PHL, which correlates with the already published reports **(Figure 12 a)**. DSC thermogram of SBE-*β*-CD represents a broad endothermic peak

and sharp endothermic peak 258.21 °C attributed to the dehydration and decomposition of SBE-*β*-CD. In the thermogram of PM, a broad peak was observed which might be due to loss of water molecules from CD. In addition, a less intense peak (near melting point of PHL) was also observed indicating presence of free PHL crystals in PM. Conversely, in IC thermogram, the endothermic peak of PHL melting at 269.12 °C was completely vanished, indicating apparent inclusion of PHL in SBE-*β*-CD cavity.

6.11.3. Thermal gravimetric analysis (TGA)

The degradation behavior of PHL, SBE-*β*-CD-IC and PM were characterized by TGA curves **(Figure 12 b).** The PHL displayed a single step decomposition that began at about 250.10 °C and reached its maximum decomposition rate at about 350.83 °C. At 700 °C, about 35% of the original sample was still present as a charred residue [40]. The thermal heating of SBE-*β*-CD showed two distinct phases of weight loss due to dehydration (water loss, 30 to 115 °C) and degradation (267 °C to 430 °C). TGA pattern of PM and IC demonstrated multiple step weight loss; dehydration of water embedded in CD cavity, and deterioration of PHL and SBE-*β*-CD, respectively. Although, it should be notable that, the weight loss attributed to the dehydration of water molecules embedded in CD cavity (i.e., first stage of weight loss) is relatively lower in case of IC (6.17%) as compared to PM (9.01%) and SBE-*β*-CD (11.09%). The relatively low weight loss at the first stage in case of IC was due to replacement and release of water molecules from the hydrophobic cavity of SBE-*β*-CD by PHL during incubation period and lyophilization process.

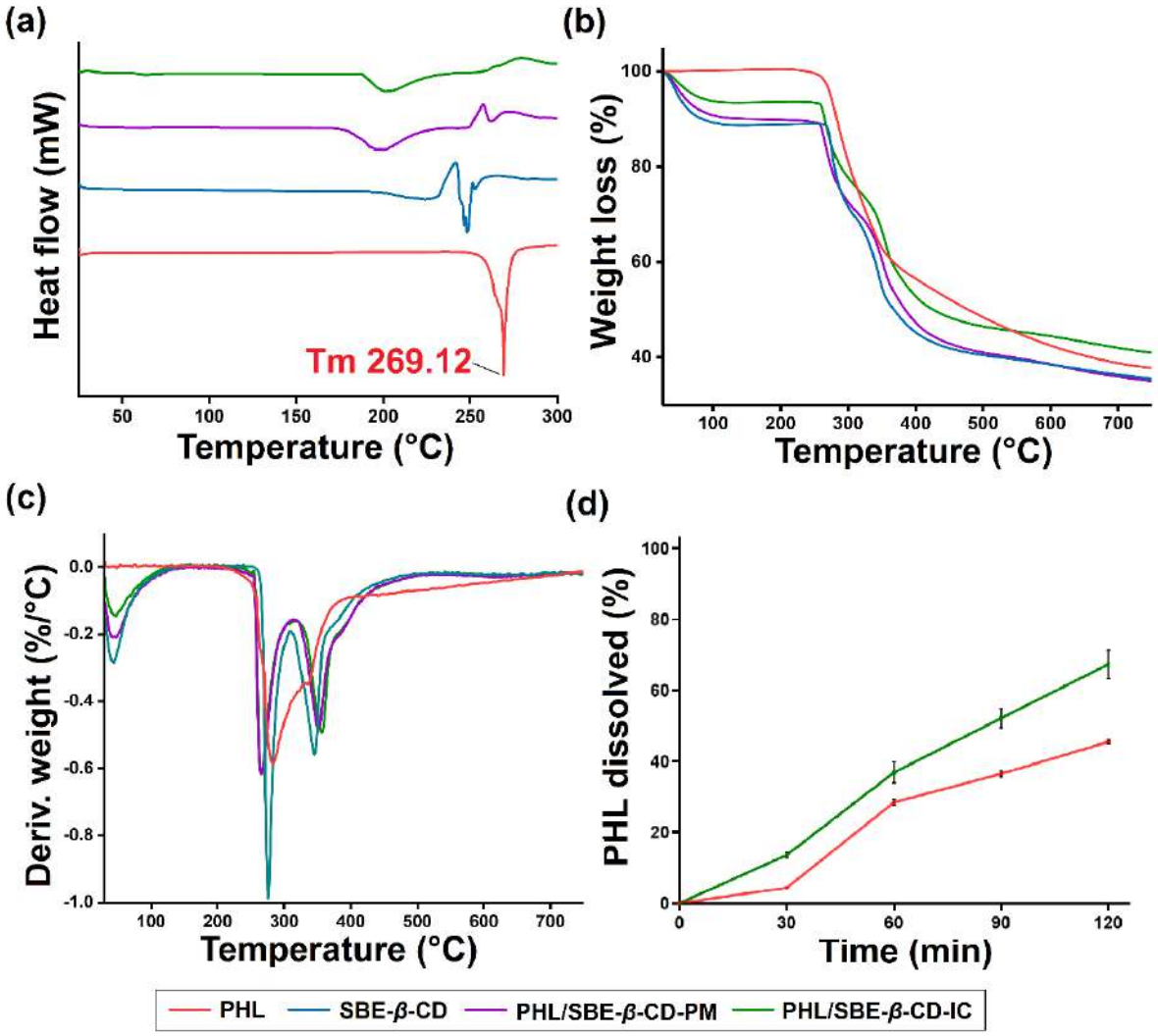

Figure 12: Thermal behavior analysis and *in vitro* dissolution profile of inclusion complex (a) DSC thermograms, (b) TGA thermograms and (c) DTA thermograms of PHL, SBE-*β*-CD, PHL/SBE-*β*-CD and physical mixture (d) *In vitro* dissolution profile of PHL and PHL/SBE-*β*-CD inclusion complex at physiological condition. The results were expressed as the mean values ± SD; n=3.

In particular, it was found that the thermal degradation of PHL in PHL/SBE-*β*-CD was pushed to a little higher temperature, from 250.10 ° to 275.31 °C, in both the TGA curves and the derivative DTG graph **(Figure 12 c)**.

6.11.4. *In vitro* dissolution study

The *in vitro* dissolution profiles of PHL demonstrated ~42% dissolution after 120 min. In contrast, freeze dried IC of PHL demonstrated ~65% of PHL dissolution after similar time point **(Figure 12 d)**. The ~1.5-folds increment in dissolution profile of PHL from inclusion complex was due to solubilization effect of SBE-*β*-CD, transformation of PHL crystalline phase to more soluble amorphous state (as evident from SEM, PXRD and DSC studies) and formation of non-covalent interactions (including van der Waals, electrostatic, hydrogen bonding and hydrophobic interactions) between the host and guest molecules.

6.12. Anti-tumor activity of PHL/SBE-*β*-CD-IC

6.12.1. CCK-8 cell viability assay

The cell viability was investigated to evaluate the enhanced *in vitro* antitumor efficacy of PHL/SBE-*β*-CD-IC in comparison to free PHL. The results reveals that PHL/SBE-*β*-CD-IC exerts significantly stronger inhibitory effects on both the cancer cell lines as compared to free PHL. More specifically, The PHL demonstrated IC_{50} value of 198.91 ± 6.6 µM in MiaPaCa–2 cells. In contrast, PHL/SBE-*β*-CD-IC demonstrated strong inhibitory effect with IC50 values of 135.58 ± 6.7 µM on MiaPaCa–2 cells **(Figure 13 a).** Similar results were observed with A549 cells, where PHL exerts relatively weak inhibitory effect compared with PHL/SBE-*β*-CD-IC with IC50 value of 172.83 ± 1.4 µM and 111.51 ± 1.6 µM, respectively **Figure 13 b).** The strong inhibitory effects of freeze-dried PHL/SBE-*β*-CD-IC on both cell lines might be attributed to the higher solubilizing effect provided by SBE-*β*-CD and enhanced cellular internalization/uptake. Moreover, it is important to note that SBE-*β*-CD in its native has negligible cytotoxic effect upto 1mM concentration on both cell lines (data not shown).

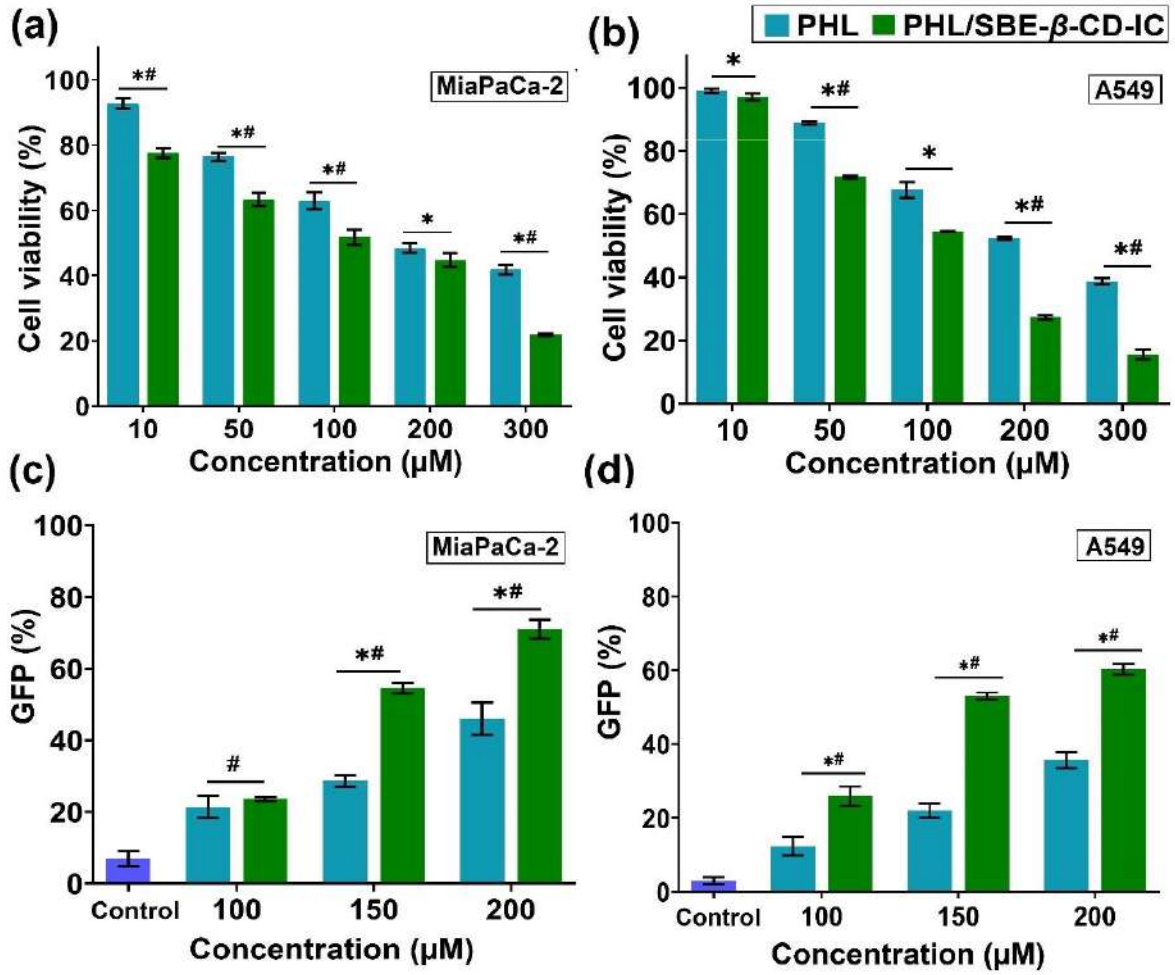

Figure 13: Dose dependent cytotoxic effect of PHL and PHL/SBE-*β*-CD inclusion complex assessed on cancer cell lines upon 24 h treatment. Cell viability graph upon treatment of PHL and PHL/SBE-*β*-CD inclusion complex in (a) MiaPaCa-2 and (b) A549 cell lines. Caspase 3/7 analysis on (c) MiaPaCa-2 and (d) A549 cells to assess the apoptotic activity of inclusion complex after 24 h treatment. Data presented as mean ± SD, n=3. *p<0.05 represent significant difference between the mean of all groups with respect to control. # p<0.05 represent significant difference between the mean of PHL concentration with respective inclusion complex concentrations.

6.12.2. Caspase 3/7 activity

Apoptosis (programmed cell death) is an inbuilt biological cell death process caused by specific cellular signalling mechanisms. Several diseases including cancers, autoimmune and degenerative conditions may result from anomalies in the regulation of cell death. Caspases (cysteine aspartate-specific proteases) are classified into two

categories: initiator caspases [caspase -2, -8, -9, -10, -11, and -12) and effector caspases (caspase -3, -6, and -7). The initiator caspases initiate downstream apoptosis signalling by the proteolytic cleavage of effector caspases for their activation. As a consequence, intracellular proteins are proteolytically degraded by active effector caspases, which leads to programmed cell death.

Thus, to establish the apoptotic procedure generated by the PHL/SBE-*β*-CD-IC, the effector caspase activity was assessed using the Cell Event™ Caspase-3/7 Green Detection kit. The detection kit reagent is composed of four-amino acid peptide (DEVD) that is conjugated to a nucleic acid – binding dye. In non-apoptotic cells, the reagents are non-fluorescent. But during apoptosis, active caspases 3 and 7 cleave the DEVD peptide, allowing the dye to attach with DNA which triggers a vibrant green fluorogenic response as indicator of apoptosis. The results demonstrated that both PHL and PHL/SBE-*β*-CD-IC treated cell lines cause caspase-mediated cell death in a concentration-dependent manner. Additionally, comparative studies represent that inclusion complex of PHL induce apoptosis more efficiently than native PHL. More specifically, it was observed that PHL/SBE-*β*-CD-IC demonstrated higher apoptosis inducing-potential (73.66 ± 1.17 %) in MiaPaCa–2 cells **(Figure 13c)** compared to A549 cells (59.01 ± 2.64 %) at highest PHL concentration (200 µM) (**Figure 13 d).** Therefore, it could be postulated that PHL/SBE-*β*-CD inclusion complex triggered cell apoptosis by activating caspase 3/7 apoptotic pathway and it may be the possible mechanism behind anti-proliferative activity of the complex.

6.12.3. Reactive oxygen species (ROS) generation by PHL/SBE-*β*-CD-IC

ROS plays crucial role in cell signalling and regulation of apoptotic signaling pathways mediated by death receptors, the mitochondria, and the endoplasmic reticulum. The

data demonstrated concentration-dependent accumulation of ROS in both the cell lines. In MiaPaCa-2 cells inclusion complex of PHL demonstrated 37.65%, 79.77% and 123.73% increase in ROS generation, whereas, in A549 cells ROS production was observed to be 55.83%, 129.61% and 192.20% (at PHL concentrations of 100, 150 and 200 µM, respectively) in contrast to untreated cells (control) as visualized from microscopic images and fluorescence intensity **[Figure 14].** The enhanced green fluorescence intensity on treatment with higher concentration of PHL and IC demonstrates high intracellular ROS generation.

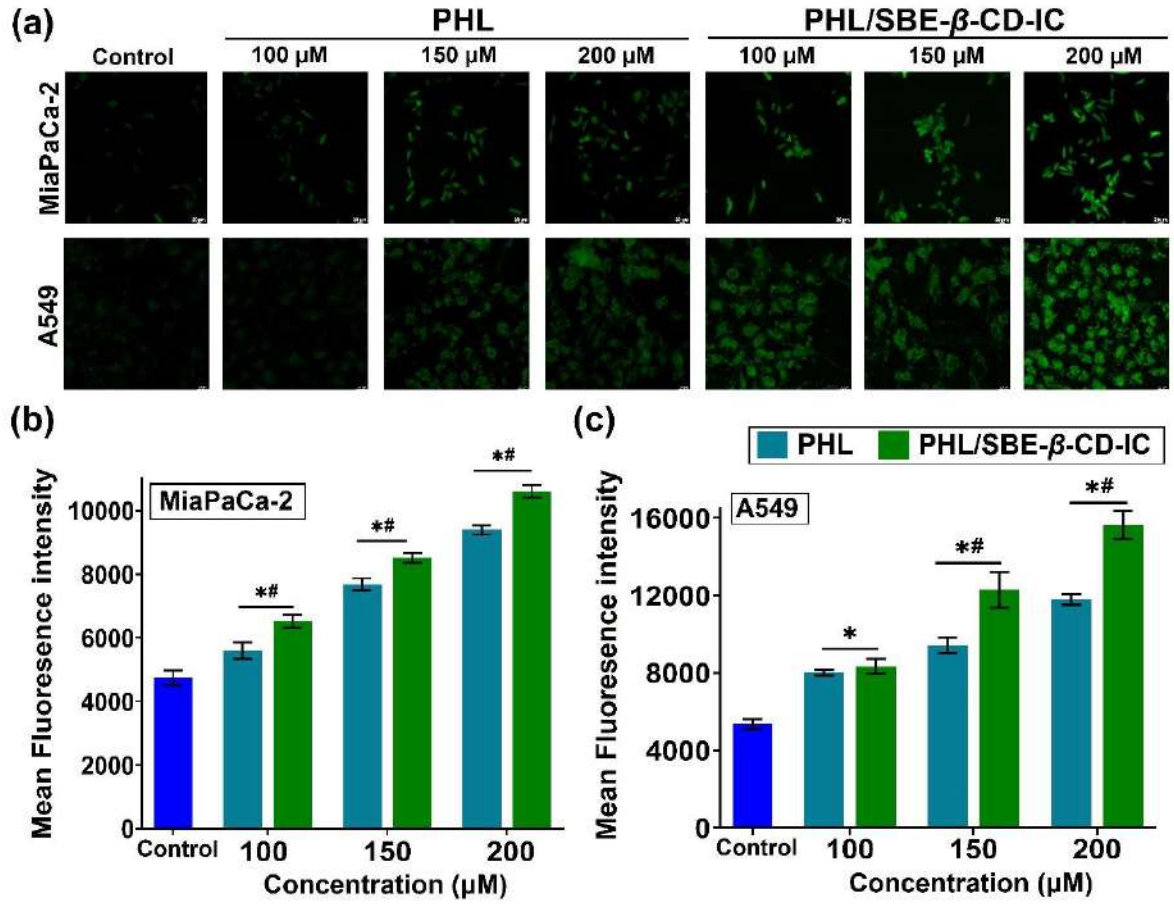

Figure 14: Reactive oxygen species (ROS) accumulation after treatment with various concentration of PHL and PHL/SBE-*β*-CD inclusion complex was observed in both MiaPaCa-2 and A549 cells (a) Microscopy images of detection of intracellular ROS generation in MiaPaCa–2 and A549 cells; Quantitative analysis of accumulation of ROS in (b) MiaPaCa-2 and (c) A549 cells respectively. Data presented as mean ± SD, n=3. *p<0.05 represent significant difference between the mean of all groups

with respect to control. # $p<0.05$ represent significant difference between the mean of PHL concentration with respective inclusion complex concentrations.

6.12.4. PHL/SBE-*β*-CD-IC induced MMP depolarization

The disruption of MMP is associated with the intrinsic apoptotic pathway. Cancer cells progressing towards apoptosis contain j monomers that generate green fluorescence, while, healthy cells have healthy mitochondria and contains j aggregates that emit red fluorescence. Increased mitochondrial permeability and changes in mitochondrial membrane potential are shown by alterations in the fluorescence intensity of JC-1 ratio of j aggregates to j monomer. The JC-1 dye staining experiment was used to assess the impact of IC on the mitochondrial membrane potential. Our results and image captured clearly demonstrated that treatment of PHL/SBE-*β*-CD-IC provoked significantly higher depolarization in mitochondrial membrane potential as compared to free PHL as the ratio of j aggregates to j-monomers was higher in both A549 and MiaPaCa–2 cells **(Figure 15).** In addition, treatment of PHL/SBE-*β*-CD-IC (equivalent to 200 µM PHL) results in ~11 folds and ~7 folds reduction in the j aggregate/j monomer ratio in MiaPaCa-2 and A549 cells respectively**.** The reduction in j aggregate/j monomer ratio by inclusion complex indicates its antiproliferative effects via intrinsic apoptotic pathway associated to disturbance in MMP.

7. Statistical analysis

Each experiment was conducted in triplicate, and finding were presented as mean ± standard deviation. The one-way analysis of variance (ANOVA) and Tukey's post hoc test were utilized in a statistical significance test using the GraphPad Prism 9 programme (GraphPad Software Inc, CA, USA). The values having $P < 0.05$ were considered as the significant between PHL and PHL/SBE-*β*-CD-IC.

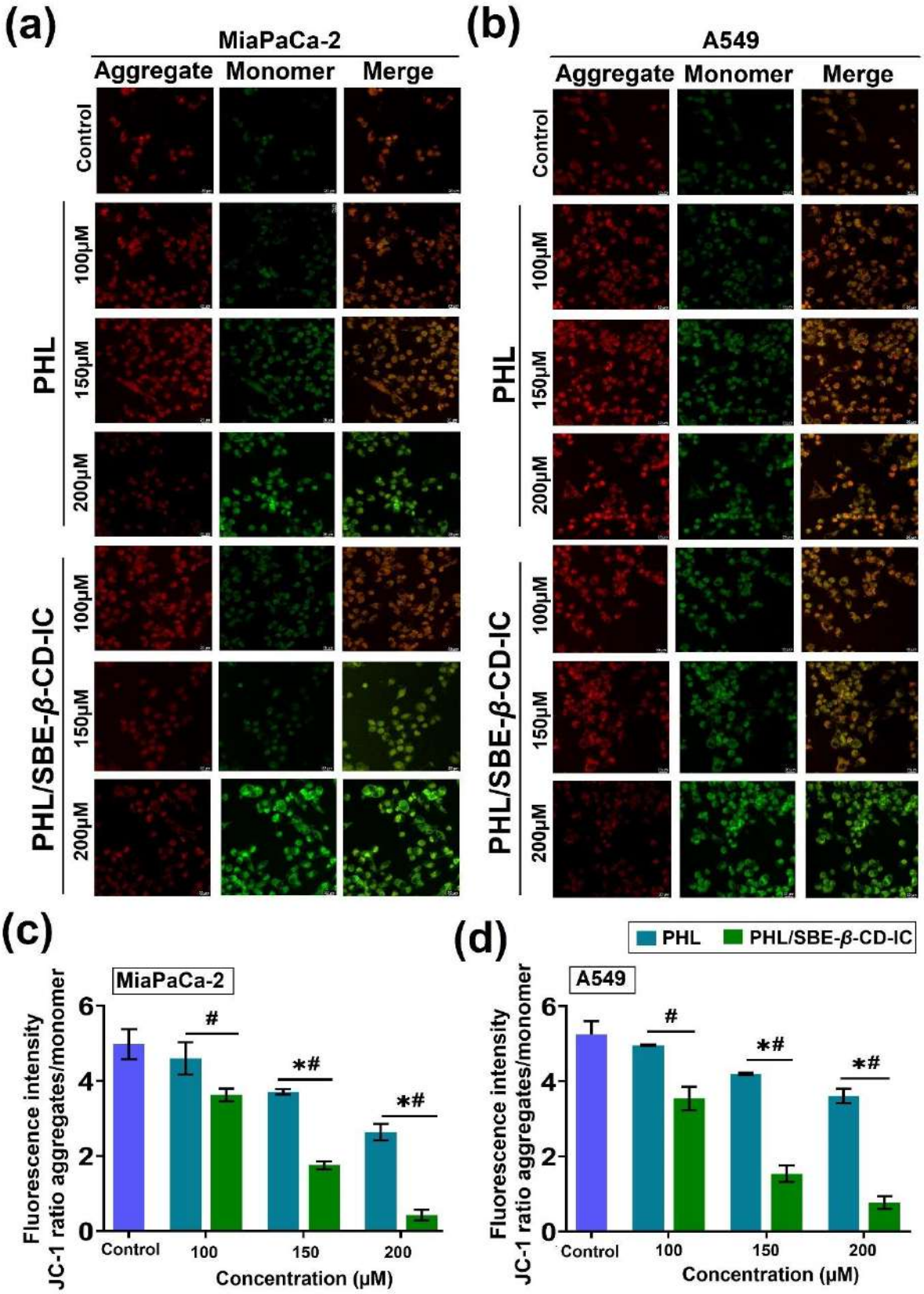

Figure 15: Determination of mitochondrial membrane potential of (a) MiaPaCa-2 and (b) A549 cells after treating them with phloretin and PHL/SBE-*β*-CD inclusion complex was assessed via JC-1 staining; The quantification of change in fluorescence intensity of JC-1 dye was performed using ImageJ software (version1.53e) in (c) MiaPaCa-2 and (d) A549 cells. The reduction in j aggregate/j monomer

ratio by inclusion complex indicates its antiproliferative effects via intrinsic apoptotic pathway associated to disturbance in MMP. Data represented mean ± SD, n=3. *****p<0.05 represent significant difference between the mean of all groups with respect to control. **#** p<0.05 represent significant difference between the mean of PHL concentration with respective inclusion complex concentrations.

8. Conclusion

In this study, we successfully developed inclusion complexes (ICs) for two bioactive molecules, phloretin (PHL) and genistein (GEN), using different derivatives of *β*-cyclodextrins (*β*-CDs) to enhance their solubility and potential applications. PHL was complexed with sulfobutyl ether-*β*-cyclodextrin (SBE-*β*-CD) through lyophilization, while GEN was complexed with hydroxypropyl-*β*-cyclodextrin (HP-*β*-CD) and methyl-*β*-cyclodextrin (M-*β*-CD) using spray drying.

Solid-state characterizations (FTIR, DSC, TGA, PXRD, and SEM) for both PHL and GEN ICs provided strong evidence of their encapsulation within the CD cavities. The molecular interactions were further confirmed by 1H NMR and 2D-NOESY analyses, revealing the specific orientation of PHL and GEN within the CD cavities. PHL's aromatic hydroxyphenyl ring (ring A) was inserted into the SBE-*β*-CD cavity, while GEN's hydroxyphenyl and chromone rings were encapsulated within the M-*β*-CD and HP-*β*-CD cavities, respectively. These interactions resulted in significant chemical shift variations, indicating successful inclusion.

The in vitro dissolution test of the PHL/SBE-*β*-CD-IC showed an improved dissolution profile compared to free PHL, while in vitro cytotoxicity assays demonstrated enhanced antiproliferative activity against MiaPaCa-2 and A549 cells. This was attributed to increased caspase 3/7 activation, ROS generation, and disruption of mitochondrial membrane potential.

For GEN, molecular modeling and MD simulations supported the experimental findings, showing stronger interactions and lower binding free energy with M-*β*-CD compared to HP-*β*-CD. The thoughtful combination of experimental and computational analyses provided detailed insights into the different binding modes and orientations of GEN within the CD cavities. Overall, the findings of this study suggest that forming ICs with *β*-CD derivatives is a promising strategy for enhancing the solubility, stability, and bioactivity of hydrophobic bioactive molecules like PHL and GEN. These ICs have potential applications in the food, nutraceutical, and pharmaceutical sectors.

9. Impact of the research in the advancement of knowledge or benefit to mankind

The research presented in this study significantly advances the field of drug delivery and functional food development by addressing the challenges associated with the poor solubility and bioavailability of hydrophobic bioactive molecules like phloretin (PHL) and genistein (GEN). By successfully developing inclusion complexes with modified *β*-cyclodextrins such as Captisol® (Sulfobutylether-*β*-cyclodextrin), which is already utilized in 15 (FDA approved) marketed products, this work not only underscores the versatility and potential of cyclodextrin-based systems but also paves the way for expanding the application of these systems in pharmaceuticals, functional foods, and nutraceuticals. This work lays a solid foundation for the broader application of these bioactive molecules in various industries, including both pharmaceuticals and nutraceuticals. The ability to improve the bioavailability of such compounds through relatively simple yet effective techniques could lead to the development of more potent, accessible, and safer therapeutic agents, ultimately benefiting public health and contributing to the advancement of knowledge in drug delivery systems. Additionally, this research opens new avenues for the use of natural compounds in functional foods, promoting healthier dietary options and enhancing the overall well-being of individuals worldwide.

10. Literature reference

1. Dhritlahre, R. K., Ruchika, Padwad, Y., & Saneja, A. (2021). Self-emulsifying formulations to augment therapeutic efficacy of nutraceuticals: From concepts to clinic. *Trends in Food Science & Technology, 115*, 347-365.
2. Xin, X., Chen, C., Hu, Y.-Y., & Feng, Q. (2019). Protective effect of genistein on nonalcoholic fatty liver disease (NAFLD). *Biomedicine & Pharmacotherapy, 117*, 109047.
3. Nazari-Khanamiri, F., & Ghasemnejad-Berenji, M. (2021). Cellular and molecular mechanisms of genistein in prevention and treatment of diseases: An overview. *45*(11), e13972.
4. Wang, Y., Li, D., Lin, H., Jiang, S., Han, L., Hou, S., Lin, S., Cheng, Z., Bian, W., Zhang, X., He, Y., & Zhang, K. (2020). Enhanced oral bioavailability and bioefficacy of phloretin using mixed polymeric modified self-nanoemulsions. *Food Science and Nutrition, 8*(7), 3545-3558.
5. Behzad, S., Sureda, A., Barreca, D., Nabavi, S. F., Rastrelli, L., & Nabavi, S. M. (2017). Health effects of phloretin: from chemistry to medicine. *Phytochemistry Reviews, 16*(3), 527-533.
6. Gu, L., Sun, R., Wang, W., Xia, Q. J. C., & Lipids, P. o. (2022). Nanostructured lipid carriers for the encapsulation of phloretin: Preparation and in vitro characterization studies. *242*, 105150.
7. Zafar, A., Alruwaili, N. K., Imam, S. S., Alsaidan, O. A., Alkholifi, F. K., Alharbi, K. S., Mostafa, E. M., Alanazi, A. S., Gilani, S. J., Musa, A., Alshehri, S., Rawaf, A., & Alquraini, A. (2021). Formulation of Genistein-HP β Cyclodextrin-Poloxamer 188 Ternary Inclusion Complex: Solubility to Cytotoxicity Assessment. 13(12), 1997.
8. Danciu, C., Soica, C., Oltean, M., Avram, S., Borcan, F., Csanyi, E., Ambrus, R., Zupko, I., Muntean, D., Dehelean, C. A., Craina, M., & Popovici, R. A. (2014). Genistein in 1:1 inclusion complexes with ramified cyclodextrins: theoretical, physicochemical and biological evaluation. Int J Mol Sci, 15(2), 1962-1982.
9. Cid-Samamed, A., Rakmai, J., Mejuto, J. C., Simal-Gandara, J., & Astray, G. J. F. C. (2022). Cyclodextrins inclusion complex: Preparation methods, analytical techniques and food industry applications. *Food Chemistry, 384*, 132467
10. Suvarna, V., Gujar, P., & Murahari, M. (2017). Complexation of phytochemicals with cyclodextrin derivatives - An insight. *Biomed Pharmacother, 88*, 1122-1144.
11. Vyas, A., Saraf, S., & Saraf, S. (2008). Cyclodextrin based novel drug delivery systems. *Journal of Inclusion Phenomena and Macrocyclic Chemistry, 62*(1), 23-42.

NABAB KHAN
PhD Research Scholar
CSIR-GPAT-SRF Fellow
CSIR – IHBT, Palampur